

NASA TM-77957

NASA TECHNICAL MEMORANDUM

NASA TM-77957

SOLAR ENERGY AND THE AERONAUTICS INDUSTRY

Ladislao Benedek

NASA-TM-77957 19860017206

Translation of "Energía Solar y la Industria Aeronautica,"
Thesis, Olivos, Argentina, October 9, 1985, pp. 1-82.

LIBRARY COPY

JUL 18 1988

LANGLEY RESEARCH CENTER
LIBRARY INGA
HAMPSHIRE VIRGINIA

NATIONAL AERONAUTICS AND SPACE ADMINISTRATION
WASHINGTON, DC 20546 NOVEMBER 1985

DISPLAY 01/6/1

86N26678*# ISSUE 17 PAGE 2748 CATEGORY 44 RPT#: NASA-TM-77957 NAS
L.15:77957 CNT#: NASW-4006 85/11/00 74 PAGES UNCLASSIFIED DOCUMENT

UTTL: Solar energy and the aeronautics industry TLSP: Thesis

AUTH: A/BENEDEK, L.

CORP: National Aeronautics and Space Administration, Washington, D.C.

AVAIL:NTIS

SAP: HC A04/MF A01

CIO: ARGENTINA Transl. by The Corporate Word, Inc., Pittsburgh, Pa. Transl.
into ENGLISH of Argentinian Thesis, 9 Oct. 1965 p 1-82

MAJS: /*AERONAUTICAL ENGINEERING/*HYBRID PROPULSION/*SOLAR ENERGY/*SOLAR FLUX

MINS: / HETEROJUNCTIONS/ PHOTOELECTRIC EFFECT/ ROCKET ENGINES/ SOLAR CELLS/
SPECTRAL ENERGY DISTRIBUTION

ABA: Author

1. Report No. NASA TM-77957	2. Government Accession No.	3. Recipient's Catalog No.	
4. Title and Subtitle SOLAR ENERGY AND THE AERONAUTICS INDUSTRY		5. Report Date November 1985	
		6. Performing Organization Code	
7. Author(s) L. Benedek		8. Performing Organization Report No.	
		10. Work Unit No.	
9. Performing Organization Name and Address The Corporate Word, Inc. 1102 Arrott Bldg. Pittsburgh, PA 15222		11. Contract or Grant No. NASW-4006	
		13. Type of Report and Period Covered Translation	
12. Sponsoring Agency Name and Address National Aeronautics and Space Administration Washington, DC 20546		14. Sponsoring Agency Code	
		15. Supplementary Notes Translation of "Energia Solar y la Industria Aeronautica," Thesis, Olivos, Argentina, October 9, 1985, pp. 1-82.	
16. Abstract This report presents an introduction to the physical aspects of solar energy, incidental energy and variations in solar flux, as well as explaining the physical principles of obtaining solar energy. The history of the application of solar energy to aeronautics, including the Gossamer Penguin and the Solar Challenger is given. Finally, an analysis of the possibilities of using a reaction motor with hybrid propulsion combining solar energy with traditional fuels, as well as calculations of the proposed cycle and its mode of operation are given.			
17. Key Words (Selected by Author(s))		18. Distribution Statement Unlimited	
19. Security Classif. (of this report) Unclassified	20. Security Classif. (of this page) Unclassified	21. No. of Pages 74	22. Price

N155777
N86-26678#
NASA-HQ 2

TABLE OF CONTENTS

INTRODUCTION	4
CHAPTER 1 - SOLAR ENERGY	5
Characteristics	5
Obtaining Electrical Energy	9
CHAPTER 2 - THE FIRST SOLAR AIRCRAFT	24
Introduction	24
Gossamer Penguin	26
Solar Challenger	27
Solar HAPP	33
CHAPTER 3 - NEW SOLUTIONS	40
Introduction	40
Solar Reaction Motor	40
Additional Comments	43
APPENDIX 1 - COMPTON EFFECT	44
APPENDIX 2 - TECHNICAL DATA ON SOLAR CELLS	46
APPENDIX 3 - JOULE-BRAYTON CYCLE	50
BIBLIOGRAPHY	74

SOLAR ENERGY AND THE AERONAUTICS INDUSTRY

Ladislao Benedek

INTRODUCTION

/4*

This work consists of three principal parts. The first concerns itself with solar energy in general. This section studies the physical aspects of solar energy, the quantity of incidental energy and its spectral distribution. Also, this section analyzes the variations of solar flux due to the zenithal height of the sun, the latitude of the location, the season of the year, and the height above sea level

Then the physical principle of obtaining electrical energy is explained (photoelectric effect). After presenting the external effect, the internal effect, on which the photovoltaic cells are based, is discussed. The silicon cell, including its operation and methods of production, is studied in detail. Heterojunction cells are also explained. The chapter ends with the topics of costs and research and development trends. Concrete data concerning solar cells is given in Appendix 2.

The second part of this thesis is dedicated to the history of the application of solar energy to aeronautics. The two aircraft that completed successful flights propelled exclusively by solar cells are the Gossamer Penguin and the Solar Challenger. The latter crossed the English Channel on July 7, 1981, almost 72 years after the crossing of Louis Blériot (July 7, 1909). Solar HAPP, realized by Lockheed and NASA, is a project of greater breadth. It consists of a gigantic radio-controlled glider to be used on agricultural missions. The second chapter discusses the characteristics of the three models mentioned.

The third part, together with Appendix 3, analyzes the possibility of utilizing a reaction motor with hybrid propulsion - solar energy/fuel. Although calculations of the proposed cycle and its mode of operation are included, the hypothesis and the methodology of calculation may be questionable and should be verified. Its purpose was to support the proposed plan with a certain degree of reliability.

The first two chapters are based on the bibliography cited, while the third chapter and part of Appendix 3 is my own work.

*Numbers in the margin indicate pagination in the foreign text.

CHARACTERISTICS

1.) DEFINITIONS

- Direct Radiation (D): The solar flux which reaches a surface without dispersing while traversing the atmosphere. This radiation arrives directly from the sun and, focused by means of an optical system, gives the image of the solar disc.

- Dispersed Radiation (S): A diffused component is produced in the atmosphere by the Rayleigh dispersion (absorption of photons by atmospheric molecules and their subsequent emission in other directions. The energy of the diffused light is removed from the initial beam, which becomes weakened in the process). This radiation cannot be focused by any optical system, but it contributes to the total flux received by a certain surface.

2.) THE SOLAR CONSTANT

The solar constant is the quantity of solar energy received per unit of time and per unit of area at the median Earth/Sun distance on a surface normal to the incidental beam. This constant does not take into account losses through atmospheric effect. Its value is:

$$1353 \text{ W/m}^2$$

At sea level this value is reduced to 930 W/m², due to losses in the atmosphere.

Due to orbital eccentricity, the variation of the solar flux with respect to the median value discussed above is +3.42% and -3.27%.

3.) SPECTRAL DISTRIBUTION

The distribution of energy originating from the sun as a function of the wavelength is basically that of a blackbody at 5800 deg. K. Due to absorption by the atmosphere of certain molecular bands and to other losses, the distribution of energy received on the earth's surface is not the same. This difference can be appreciated in Figure 1.

The bands of absorption are principally those corresponding to water vapor and to carbon dioxide. The presence of ozone in the atmosphere effectively terminates the spectrum of energy received to 0.3 microns in ultraviolet, and the water vapor does the same to 20 microns in infrared.

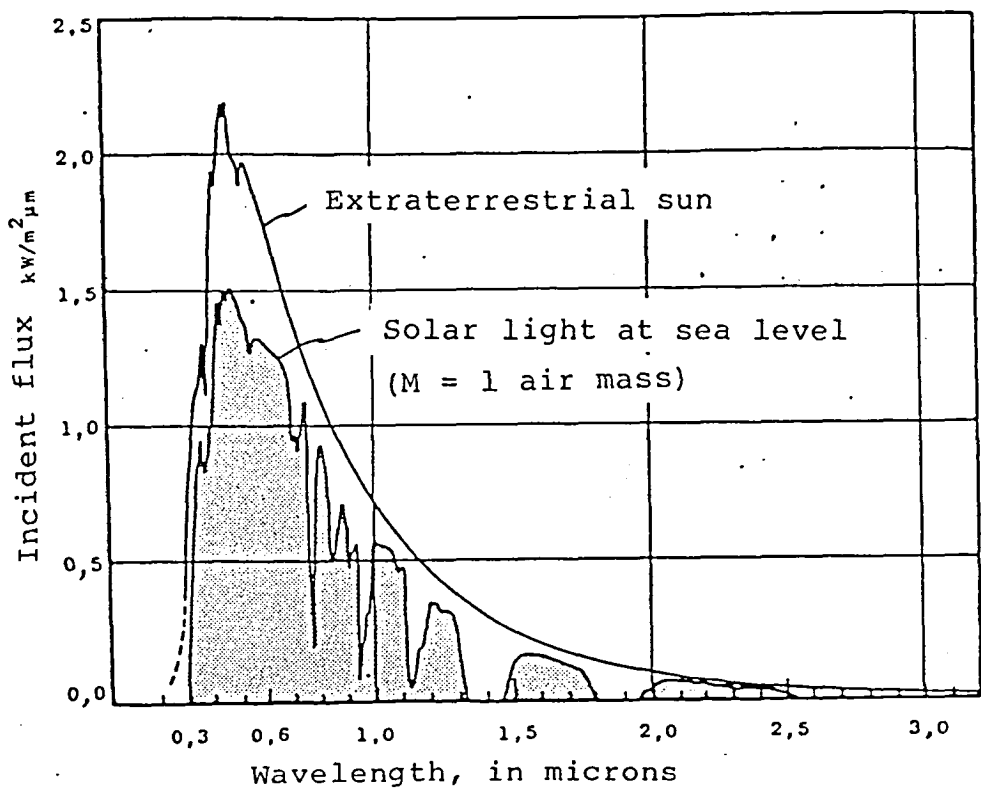


FIG. 1 SPECTRAL DISTRIBUTION OF SOLAR ENERGY WHICH REACHES THE EARTH, OUTSIDE OF THE ATMOSPHERE AND AT SEA LEVEL WITH ZENITHAL INCIDENCE (AM-1) CONTAINING 20 mm WATER VAPOR

4.) DAILY VARIATIONS IN THE SOLAR FLUX

The solar flux varies in accordance with the angular altitude of the sun and consequently to the change in the air mass through which solar light must pass.

This effect can be observed in Figure 2.

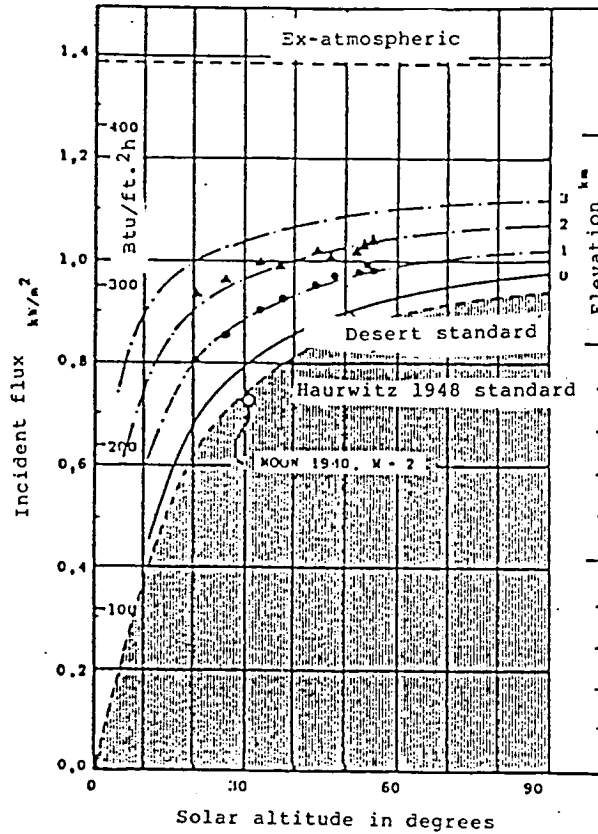
These variations may be expressed by means of the following empirical formula:

$$I (Z) = I_0 e^{-c(\sec Z)^s}$$

where $\left\{ \begin{array}{l} I_0 \text{ is the solar distance} \\ Z \text{ is the zenithal distance (angle)} \\ C = 0.357 \\ S = 0.678 \end{array} \right\}$ empirical constants

The zenithal distance is not only a function of time but it also depends on the latitude of the location and on the solar descent. This can be calculated as follows:

$\cos Z = \sin \lambda \sin \delta + \cos \lambda \cos \delta \cos t$
 where λ = latitude
 δ = solar descent
 t = the hourly angle of the sun, equal to the number of hours that the sun is distant from the meridian of the location (midday).



/8

FIG. 2 VARIATIONS IN DIRECT AND NORMAL SOLAR FLUX WITH ZENITHAL DISTANCE AND ELEVATION. Measurements by Laue (1970) and standard curves by Haurwitz (1948) and Moon (1940).

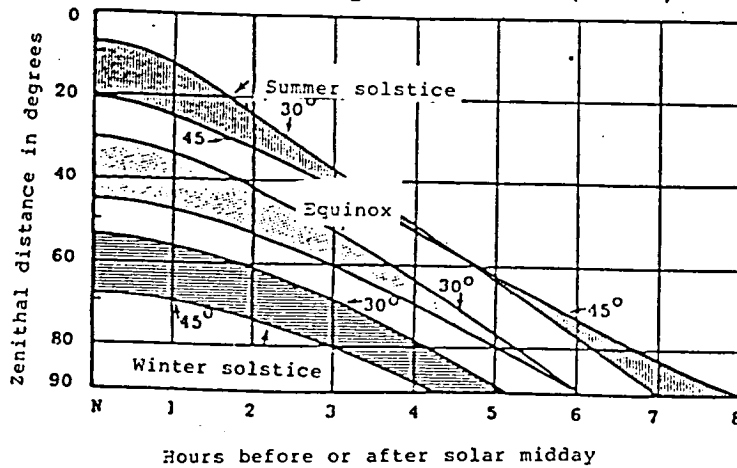


FIG. 3 VARIATION OF THE ZENITHAL DISTANCE OF THE SUN AS A FUNCTION OF TIME, FOR DISTINCT LATITUDES AND SEASONS OF THE YEAR.

5.) VARIATIONS WITH ALTITUDE

Solar flux increases with the altitude, due to which solar light must travel shorter distances within the atmosphere, and consequently suffers less absorption and diffusion.

After obtaining a series of measurements (data obtained by Laue in 1970) the following empirical equation was adjusted to them:

$$I(z,h) = I_0 (1-ah) e^{-c(\sec Z)^2} + ah I_0$$

where h is the altitude in kilometers
 $a = 0.14 \text{ km}$

Due to the lineal boundary, $(1 - ah)$, the equation is useful only for the first kilometers of altitude.

6.) ENERGY CHARACTERISTICS OF A FIXED HORIZONTAL PLANE SURFACE

The solar flux which reaches the surface, per unit of area of the surface, is given as:

$$I(c) = I(z) \times \cos Z$$

Figure 4 demonstrates the available energy for this case as a function of the latitude and the seasons of the year.

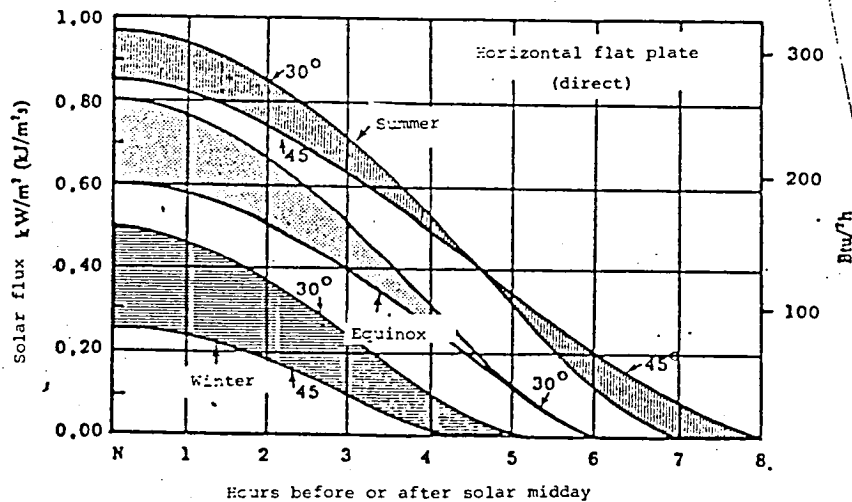


FIG. 4 VARIATION OF THE DIRECT SOLAR FLUX ON A HORIZONTAL PLANE SURFACE AS A FUNCTION OF TIME AND SEASON OF THE YEAR FOR DISTINCT LATITUDES

The daily energy received by a horizontal plane surface is as follows:

LATITUDE	ENERGY RECEIVED (kWh/day)		
	SUMMER	EQUINOX	WINTER
45 Deg.	7.54	4.31	1.23
30 Deg.	7.85	5.53	3.00

It should be noted that all the data presented correspond to energy supplied by direct radiation.

OBTAINING ELECTRICAL ENERGY

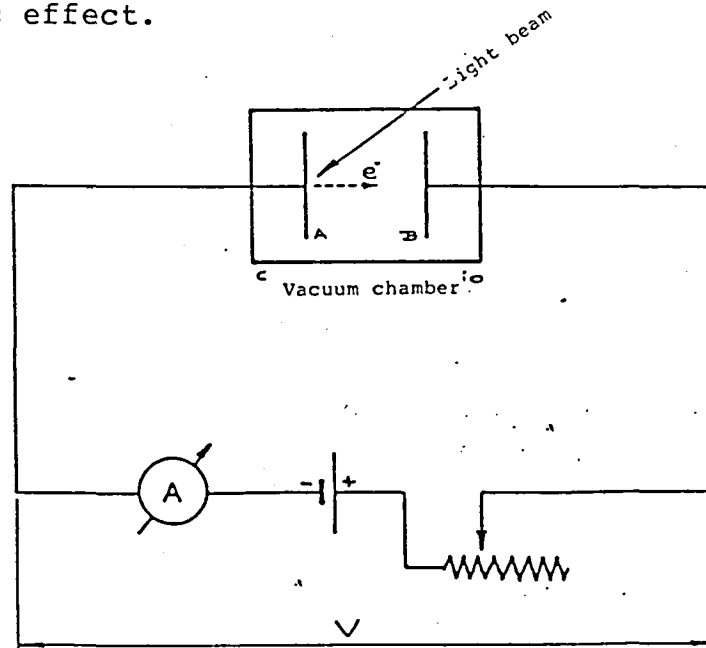
/10

1.) INTRODUCTION

There are diverse methods for usefully converting the energy which arrives in the form of solar radiation.

One of these consists of storing this energy in the form of heat and using it in a thermodynamic cycle, thereby employing it usefully. In addition to the thermal method of conversion, there are others which directly convert the electric energy received. A tension is generated within the thermoelectric cell at the union of two different metals when one of the metals is maintained at a different temperature than the other. The efficiency is low, varying between 1.8% and 2.5%.

An important method of direct obtention is that based on photoelectric effect.



A and B are Metal Plates

FIG. 5a Circuit in which Photoelectric Effect is Evident. The difference of potential between Plate A and B orients the freed electrons to give origin to the current measured by the ammeter.

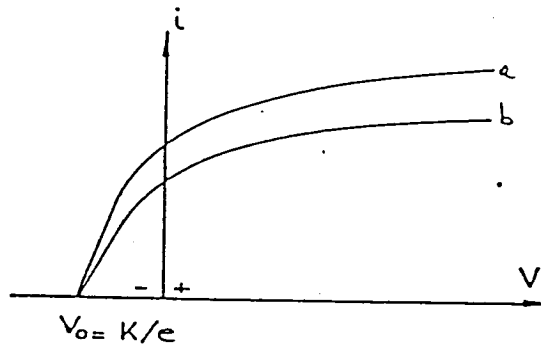


FIG. 5b INTENSITY OF CURRENT AS A FUNCTION OF THE DIFFERENCE OF POTENTIAL APPLIED TO PLATES A AND B. Before the incidence of the light beam, it can be observed that for $V = 0$, there exists a current due to the photoelectric effect. When $V = -K/e$, the difference of potential is sufficient to restrain all the electrons and prevent their reaching Plate B. Curve "a" corresponds to a greater intensity of the light beam than curve "b". For sufficiently high values of V the current stabilizes; beginning with a certain value of V all the freed electrons reach plate B.

2.) THE PHOTOELECTRIC EFFECT

If a beam of light falls on a metal sheet which might be within an electric field, such as in Figure 5, the ammeter will register a circulation of current.

This occurs because the light beam brought about the /11 liberation of some electrons which were able to escape from the metal when energy was transferred to them.

The energy attracted by one photon is:

$$E = h\nu$$

Where $h = 6.63 \times 10^{-34}$ J.s (Planck constant)

ν = frequency of the photon.

An electron requires a minimum amount of energy, E_0 , to overcome the potential barrier which exists on the surface of the metal. If $h\nu$ is greater than E_0 , then an electron can absorb sufficient energy to be able to escape from the metal. The surplus energy is transmitted to the electron in the form of kinetic energy. This value, K , is only a maximum value, as the electron may lose part of this energy in internal collisions before leaving the metal.

$$K = h\nu - E_0$$

It is important to note that K does not depend on the intensity of the light beam, since it does not depend on the quantity of incidental photons, but on the energy of each one of these. To duplicate intensity means duplicating the quantity of electrons expelled from the metal, with a maximum kinetic energy, K .

If $h\nu$ is less than E_0 , no electron can leave the metal independently of the intensity of the incident beam.

<u>MATERIAL</u>	<u>E_0 (eV)</u>
Sodium	2.3
Aluminum	4.2
Lithium	2.3

It is important to point out that the photoelectric effect, or the absorption of a photon by a completely free electron, is not possible since the equations of conservation of quantity of movement and that of energy-mass which express the relativistic equations will not be simultaneously satisfied. (See demonstration in Appendix 1).

The external effect is observed principally with metals within an area in which a vacuum has been created. The metals are very opaque to light and therefore the photon is absorbed very close to the surface. For this reason it can escape from the metal surface.

3.) INTERNAL PHOTOELECTRIC EFFECT

/12

In the internal effect certain charge carriers become freed within the recess of the material through the absorption of photons, and this can be observed principally in the semi-conductors.

These materials are more transparent to light, in such a way that the absorption of photons is produced at a greater depth and very few electrons can escape from it.

If the energy attracted by the photon is greater than E_g , tension of the empty band of the semiconductor, then a empty-electron cell is created. These carriers are free to move within the conduction band for a certain time, the "life period", during which they have travelled a certain distance termed the "length of diffusion". In order for a current to exist, there must be an electrical field. This is achieved by creating a junction between semiconductor materials. The junction may be of the p-n type, by doping the base material with certain impurities, or it may be a direct junction with different materials (heterojunction).

When the electrical field is created the junction causes the electrons to shift to one direction and the empty electrons

to move in the opposite direction. The passage of a current can be observed by joining the sides of the junction with a conductor.

4.) THE SILICON SOLAR CELL

Figure 6 shows a section of a solar cell, in this case doped with silicon.

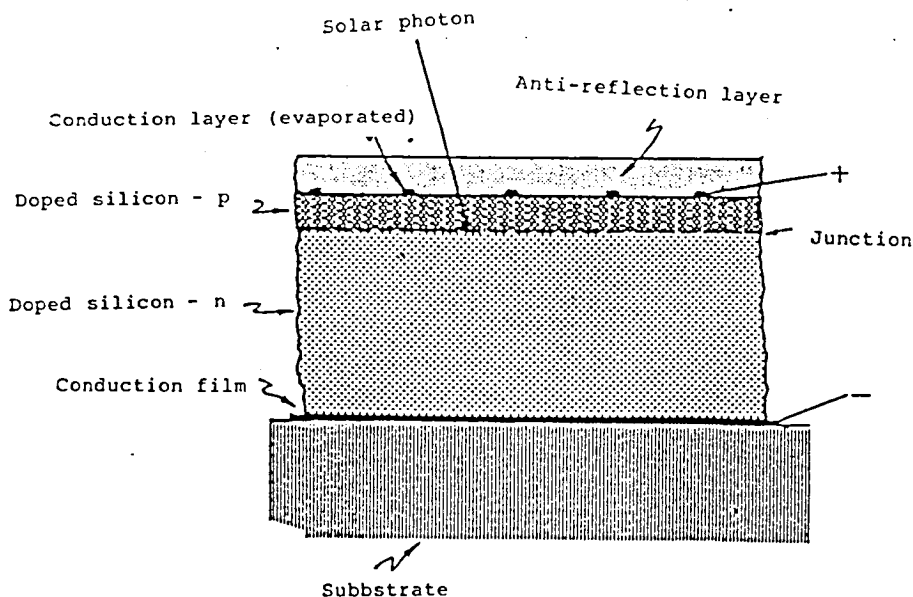


FIG. 6 SCHEMATIC SECTION OF A SILICON SOLAR CELL (P-N).

The top layer is formed by very pure silicon, doped with /13 boron, in order to obtain type-p silicon. Boron has three (3) valence electrons. Upon forming part of the silicon network (four (4) valence electrons), "empty" spaces remain in the place which should have been occupied by the fourth electron, which does not exist in boron. This empty space is replaced by the positive carrier.

The bottom layer is the same silicon doped with arsenic, producing type-n silicon. Contrary to what happened with the boron, there is an excess of electrons in this zone since arsenic has five (5) valence electrons and uses only four (4) for covalent bonds with the silicon atoms.

In this case we have one solar cell with a p-n junction.

When a photon is absorbed, an empty-electron cell is /14 formed (caused by an electron from valent band jumping to the conduction band). If the crystalline structure is very pure, the "life" of the cell is high. If instead there are areas of structural impurities or imperfections, such as the limit between two crystals of the material, its "life" decreases.

Therefore, the perfection and purity of the crystal are very necessary for obtaining adequate efficiency.

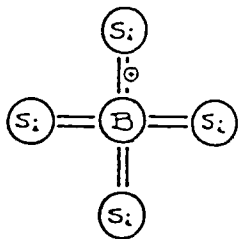


FIG. 7a SILICON DOPED WITH BORON
Lack of an electron causes an "empty space" (positive carrier) in the covalent bond. If a free electron occupies the space, the structure remains negatively charged.

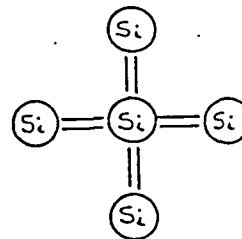


FIG. 7b STRUCTURE OF SILICON
The structure is basically neutral. The escape of an electron from the covalent bond (band of valence), to the conduction band (free electron) causes an empty electron cell.

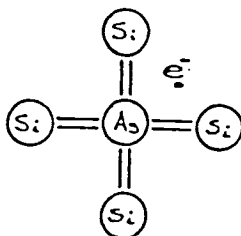
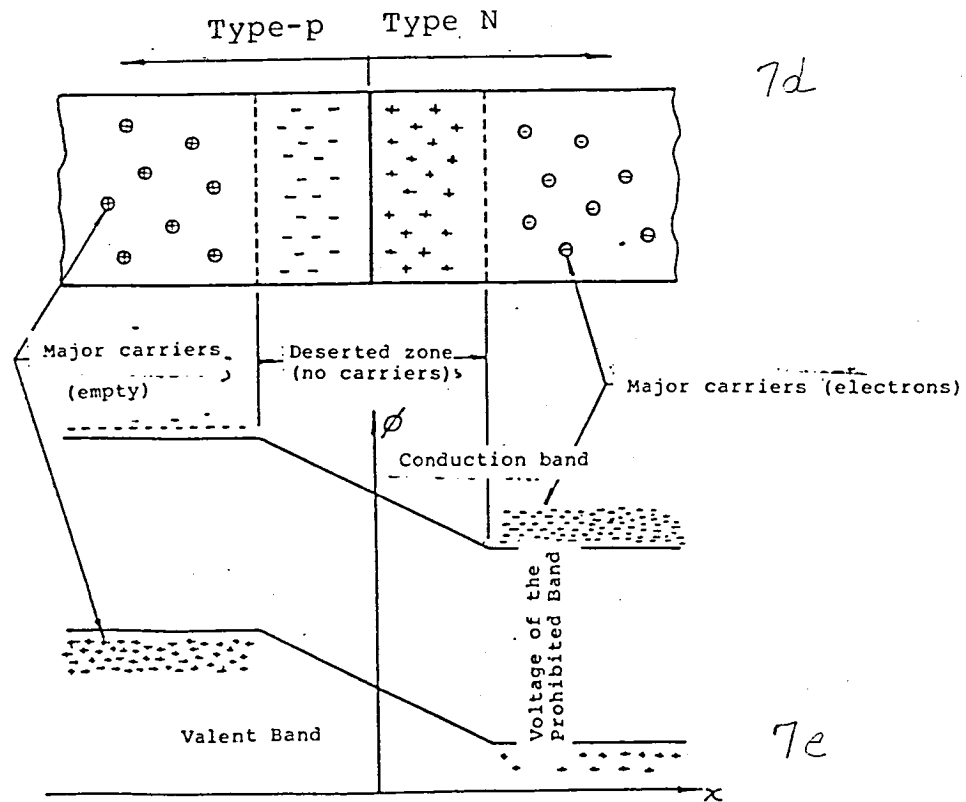


FIG. 7c SILICON DOPED WITH ARSENIC. The extra electron will be free (negative carrier). If the electron leaves the area, this part of the structure remains positively charged. (TYPE - N).

The p-n bond provides the electric field necessary to obtain the passage of current once the empty-electron cells have been created. The field is permanent and intense in the zone of the bond where the electrons are swept to one side and the empties on the other. The bond and its field occupy a very narrow thickness, and its influence over the carrier cells is reduced to a characteristic distance, called "length of diffusion". This length is the median distance which a cell may travel before being rejoined.

The thickness of the top layer, p, is about 1 to 2 microns, and the length of diffusion is from 0.1 to 0.3 microns. In order for an empty-electron cell to contribute to the photocurrent, the absorption of the photon must occur at a maximum of the "length of diffusion" of the bond, since otherwise the cell will be rejoined before it can be separated by the electrical field of the bond.



(top)

FIG. 7d DIAGRAM OF THE p-n BOND. The "excess" electrons in the type-n structure tend to occupy the empty spaces of the silicon doped with boron (type-p). When this happens, the potential of zone p increases, and the potential of zone n decreases. An equilibrium is reached when the potential barrier is such that it stops the passage of electrons from zone-n to zone-p. In the region of the bond there remains a "deserted" zone since it lacks carriers (free and empty electrons). A high potential field, $\Delta V / \Delta x$, exists in this zone, since the value of Δx is very small. This great potential field sweeps the empty-electron cell created by the absorption of a photon from one side to the other.

(bottom)

FIG. 7e DIAGRAM OF THE POTENTIAL AS A FUNCTION OF ITS POSITION IN THE P-N BOND.

This implies that the actual production of current is lower than that theoretically possible, since the photons with sufficient energy will create the cell, whether or not this is useful, in order to generate the photocurrent.

The spectral sensitivity of silicon, that is the depths at which the photons of distinct wavelengths are absorbed, defines the position which the bond must occupy to obtain the maximum yield. This variation can be seen in Figure 8.

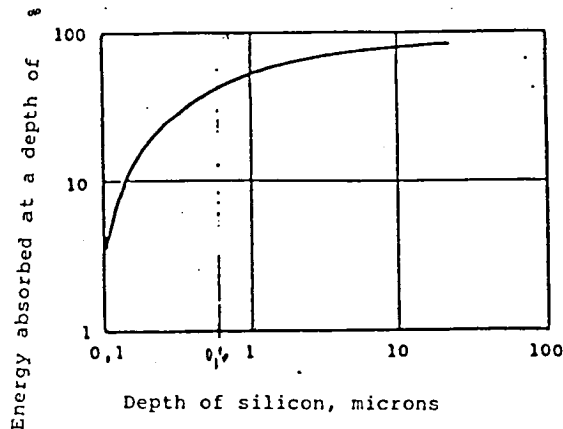


FIG. 8 SOLAR ENERGY ABSORBED BY THE SILICON AS A FUNCTION OF ITS DEPTH.

In infrared, for example, silicon is more transparent, /15 since these radiations penetrate more deeply.

5.) EFFICIENCY

Although the efficiency of the internal photoelectric effect is 100% for photons with energy greater than that of the vacuum band, we saw in the preceding section the reasons why not all of this energy can be utilized. The following table shows the actual efficiency of various cells.

Efficiency of Solar Cells

<u>Material</u>	<u>Tension of the Vacuum Band</u>	<u>Efficiency %</u>	<u>Status</u>
Si (wafer)	1.1	12-18	Commercial
Si (thin film)		2-5	Experimental
GaAs/GaAlAs	1.4	16-20	Experimental
CdS/Cu ₂ S	2.3	5-8	Advanced Development
CdTe	1.4	5-6	Experimental
SiC		1-3	Experimental
GaP	1.9	1-3	Experimental
InP	1.3	2-5	Experimental

6.) MANUFACTURING SILICON CELLS

The cost of the cells is not raised by the price of the base material, but by the cost of production. Silicon is a very abundant material, but it is not found in a pure state. Normally it is obtained from silica sand, SiO₂. This material is reduced by heating it with carbon in an electric furnace, thereby obtaining silicon with a purity of approximately 96 to 98%. Purities of 99.7% can be attained by later treatment with acids. However, this degree of purity is not sufficient for use

as a solar cell. The process for improving it is to convert it chemically into silicon tetrachloride, SiCl_4 , in order to subsequently reduce it with metallic zinc.

In this way a purity of 99.97% is obtained. Later, purification is achieved through the growth of a silicon crystal by the CZOCHRALSKI method, by slowly withdrawing a ball of silicon from the silicon bath. From this moment purity is no longer expressed in the form of percentage. A much more useful value is its resistivity. Silicon appropriate for use in solar cells has a resistivity on the order of $0.2 \Omega \text{cm}$.

To obtain a solar cell from pure silicon, impure substances must be added to create the p-n bond.

First, the ball of silicon is doped with arsenic to /16
create the doped product -n. The subsequent process consists of 6 principal stages:

a.) The ball is cut as thinly as possible into wafers. The thickness is normally 0.5 to 1 mm.

b.) The wafer is polished to eliminate defects in the superficial crystalline structure produced by the cutting. Then it is cleaned.

c.) Atoms of boron are diffused in order to produce the top layer of type -p, obtaining the pn bond. It must be noted that the reverse can take place, that is, that the base material may be type -p silicon and that the top surface may be doped with impurities which produce type -n silicon. It must also be noted that in addition to boron, other substances having a valence of 3, such as gallium and indium, can be used to dope the silicon to obtain type -p material.

d.) After another cleaning, the wafers are placed in the vacuum chamber, where the conduction grid is formed, depositing the metal on the surface of the cell through evaporation. A camouflage prevents the metal from depositing itself in those parts of the surface of the wafers which will be active regions.

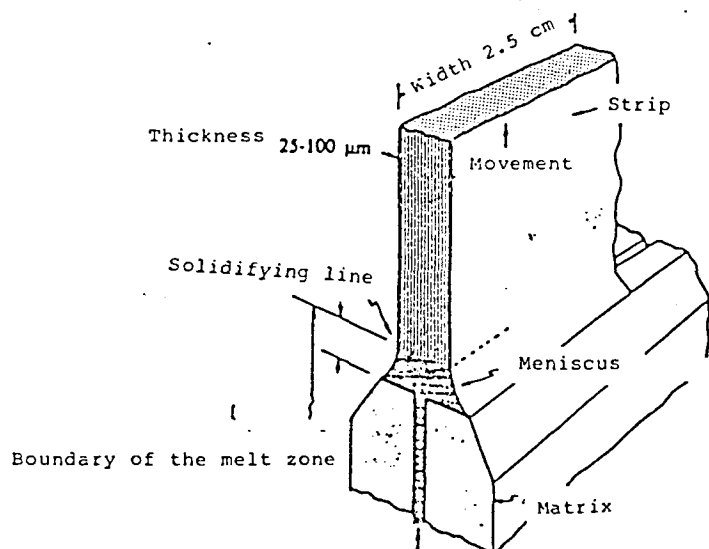
e.) The wafer is welded to the contacts of the material which will be the base or the lower part of the cell. The solar cell is complete in itself.

f.) Quality control defines the acceptance or rejection of the product which, once approved, may be installed in the desired system.

Cells having a rectangular rather than a circular shape can be manufactured for those cases where the weight of the cells is critical or in which the available surface is restricted.

Although this method of production is very reliable, it is

also very expensive. One way of lowering costs is to make the silicon crystal in the final shape which the cell will have; for example, in strips or ribbons of silicon. One of the most promising techniques is silicon EFG (edge-defined film growth). The technique was developed by Stephanov to obtain strips of germanium. Therefore this method is also known as the Stephanov method. The formation of the strip is illustrated in Figure 9.



/17

FIG. 9 DIAGRAM OF THE MOLD AND THE FILM CORRESPONDING TO THE SILICON EDGE DEFINED FILM GROWTH SYSTEM, EFG.

The silicon is extracted directly from the high-purity silicon bath using a mold in order to give it the approximate shape that the strip will have. Surface tension is such that the liquid silicon adheres to the seed crystal and to the edges of the mold. If we adjust the speed of extraction, the silicon emerges and solidifies rapidly in a strip with the dimensions of the mold, which may be around 100 microns thick, and 2 to 4 cm wide.

The disadvantage of this process is that since silicon is a very effective solvent, it is very difficult to find a material (for the mold) which does not inject undesired atoms of impurity into the strips. For this reason, the yield of the strips is very low.

7.) POLYCRYSTALLINE CELLS

Since the production cost of monocrystalline silicon cells is very high, efforts have been made to use polycrystalline cells. If the size of each crystal is sufficiently large compared with the length of diffusion, the efficiency will be approximately equal to that of a monocrystalline cell.

Polycrystalline silicon can deposit itself in many relatively inexpensive forms, such as evaporation in a vacuum, or chemical deposits of the vapor or the drippings. The real problem is finding an inexpensive substrate on which to deposit the silicon. Experiments have been done using steel and graphite as substrate materials.

The cost of the substrate materials keeps increasing, since the material must be such that the metal-semiconductor junction is adequate. Steel is inexpensive, but it injects impurities in the silicon. Isolating the cell from the substrate with a layer of evaporated silica (SiO_2) or with boronsilicated glass has been attempted. These problems were not solved and, therefore, the efficiency is low. /18

8.) HETEROJUNCTION CELLS

Of course experiments have been conducted using other types of solar cells rather than silicon (that is, with p-n junctions). The concept of heterojunction implies that the junction is not formed by the same material doped with different impurities, but that it deals with the junction between two different materials

Cadmium sulfide (CdS) cells were developed at the same time as the silicon cells, however, they soon lost the race opposite silicon. The fundamental problem was that these cells did not

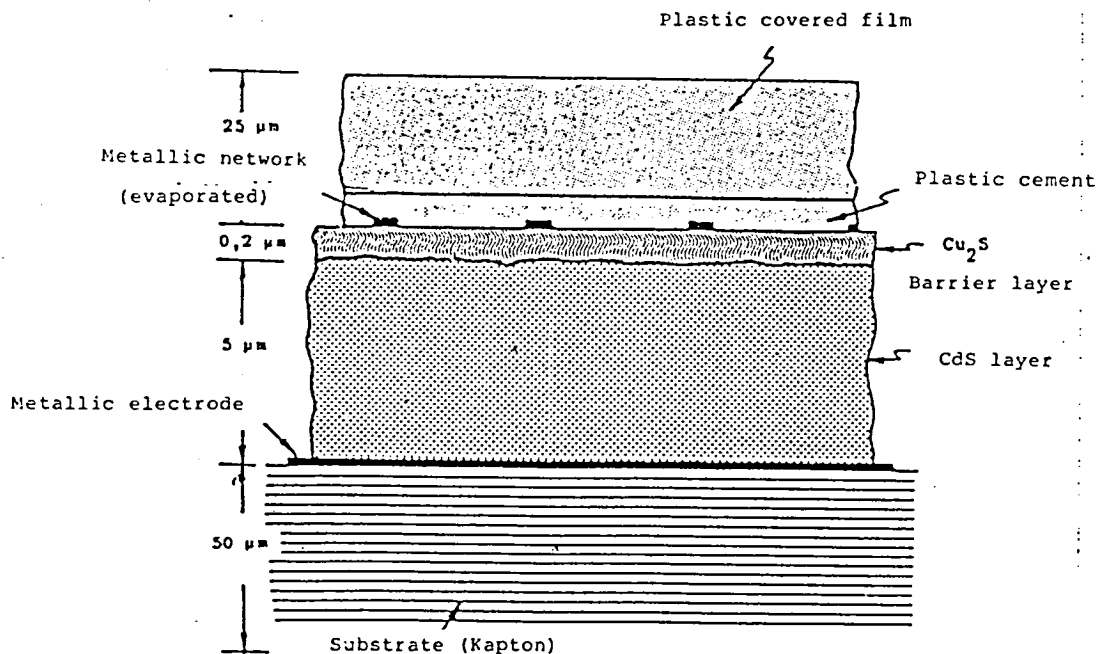


FIG. 10 DIAGRAM OF A SECTION OF A SOLAR CELL WITH A CADMIUM SULFIDE HETEROJUNCTION. (The cover may also be of glass, deposited by evaporation, and the substratum may be of a metallic laminate).

have a dependable efficiency and also tended to deteriorate in the earth's atmosphere. Their great advantage was the inexpensive production cost, and experiments are currently being conducted to improve them.

Figure 10 illustrates a section of a cadmium sulfide cell.

This is composed of a lower layer of CdS and a top layer of copper sulphide. The junction is the active region of the cell. Copper sulphide (Cu_2S) has a composition of 1.96:1 to 1.98:1, instead of a ratio of 2:1, to obtain an efficient cell. The efficiency is about 5%. These cells are very sensitive to water vapor, and therefore must be encapsulated with utmost care. It must be remembered that cadmium is toxic, thereby creating safety problems.

Another less toxic base material is zinc selenide (ZnSe), which can be used as a substitute.

These cells are constructed by means of successive evaporation of the materials on a substrate. This process requires small quantities of each material, since the thicknesses are very small; consequently more expensive materials than those used in silicon cells may be utilized.

Another type of heterojunction can be achieved with gallium arsenide (GaAs) and aluminum and gallium arsenide (GaAlAs). The great advantage in their use is that greater quantities of photons can be absorbed within the length of diffusion of the junction. Production is very expensive, but an efficiency of 20 to 28% can be attained. The manufacturing process is CVD (chemical vapor deposition).

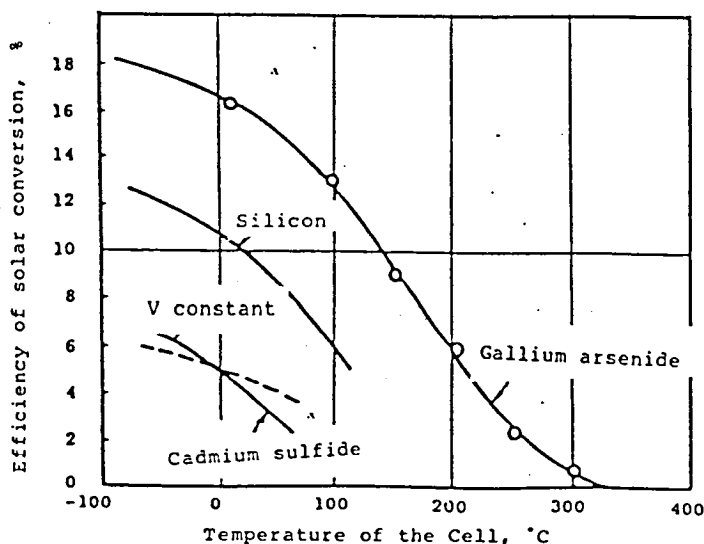


FIG. 11 VARIATION IN THE EFFICIENCY OF DIFFERENT CELLS BASED ON TEMPERATURE

9.) HEAT PERFORMANCE

The solar cells are warmed by the action of the solar flux since the empty-electron cells which are formed outside of the influence of the junction are rejoined uselessly, but they produce heat. Figure 11 shows the performance of different cells as a function of temperature.

10.) COSTS

/20

The cost of production of silicon solar cells is distributed as follows:

Solar Cells	Base material - silicon	35%
	Other materials	6%
	Labor	32%
Interconnections, Modules	Material	8%
	Labor	<u>19%</u>
		100%

It is evident that to appreciably reduce the cost, manufacturing methods must be improved to reflect a decrease in the cost of labor and the price of the base materials.

A study made by AEG-Telefunken in 1978 estimates the following evolution of costs:

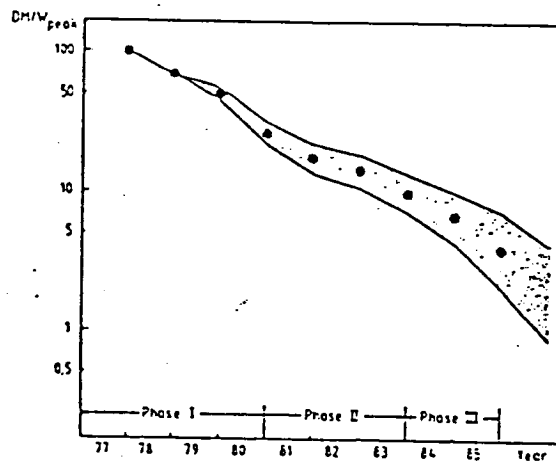


FIG. 12 EXPECTED EVOLUTION OF THE COST, IN MARKS, BY MAXIMUM POTENTIAL SUPPLIED BY A SOLAR CELL (Indications of Phase I, II and III correspond to the research and production plan established by AEG-Telefunken).

Technical data on several solar cells are grouped in Appendix 2.

Application of photovoltaic energy has enjoyed a certain popularity in recent years. This is due to the systems' great reliability and low maintenance cost. For certain specific cases even the cost of inversion is lower, as for example in water pumps in remote locations. However, the manufacture of solar cells is still too expensive for more common applications. Two trends exist in the field of research. The first consists of obtaining cells at a minimum cost, while the other seeks to obtain higher yields. The two trends are mutually exclusive only in the first instance.

According to the National Photovoltaic Program of the United States, one of the principal objectives is to produce electrical energy at a cost of \$0.065 per kWh. The production of energy at this price would transform photovoltaics into one of the competitive energy sources. New concepts have been researched, such as film cells and multiple junctions (not only one p-n junction in the cell).

The principal aspects being researched are the following:

a). Research on Materials

- Thin film with only one junction.
- High efficiency multi-junctions.
- Purification of silicon.
- Methods of production.

b). Development of the current collector system

c). Development of complete systems

- Reliability of modules.
- Methods of production.

The actual objectives of research and development formulated by The Solar Energy Research Institute are:

a.) Thin film with median efficiency and low cost. They are seeking to obtain cells whose efficiency may be from 10-15% at a price lower than \$50 per square meter. The material may be of polycrystalline silicon or hydrogenated amorphs with only one junction. Another possibility would be the utilization of heterojunctions of cadmium sulphide with impurities of selenide, indium, gallium, or tellurium. Being developed cells of (Cd,Zn) S/CuInSe₂ with a yield of 10.3%. These cells are very stable, and their improvement is actively being sought. Polycrystalline silicon cells are obtaining good results with the improvement of their method of production. Efficiencies of 17% have already been reached in experimental cells. It is hoped that in 1987 a series of cells having an efficiency of 15% can be produced. /22

b) Cells having a low cost and high performance. It is hoped that solar cells having an efficiency of 15-25% at a cost of around \$50 per square meter can be attained. One of the methods to be researched is the utilization of 2 or 3 superimposed junctions to achieve a better exploitation of the spectre of energy received. Work is being done on amorphous silicon alloys and with heterojunctions. The base material for heterojunction cells is gallium arsenide. Work is also being done with cadmium tellurium and copper and indium selenide (CuInSe₂). Cells of AsGa 5 microns thick with efficiencies of 18.6% have already been attained.

At the Massachusetts Institute of Technology, a type of cell was manufactured using a new concept. These are cells with a "back-surface field". The energy diagram of the junction can be seen in Figure 13. The second junction increases the prohibited band, that is the range of prohibited energy between the conduction and valent electrons. This junction acts as a mirror to the minority carriers (electrons, in the case of Figure 13). Consequently, rejoining speed is decreased, and the characteristic length or the effective zone increases to produce the separation of the empty-electron cell which finally generates the photovoltaic current.

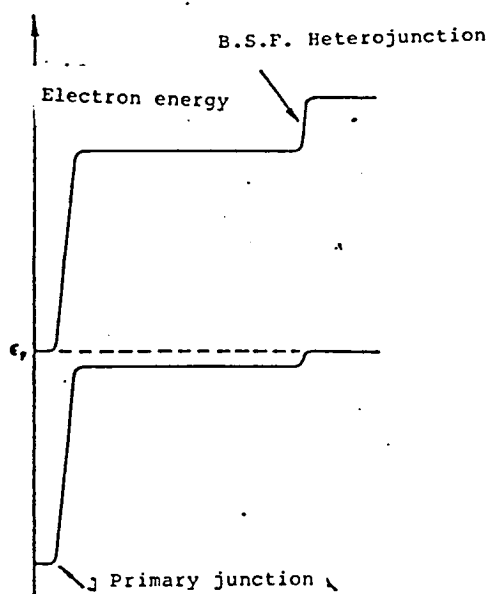


FIG. 13 SCHEMATIC DIAGRAM OF THE ENERGY BANDS OF AN n/p/p⁺ CELL WITH ONE SURFACE JUNCTION AND ONE HETEROJUNCTION.

The structure of this cell is:

/23

n - GaAs/p-GaAs/Al_{0,2}Ga_{0,8}As

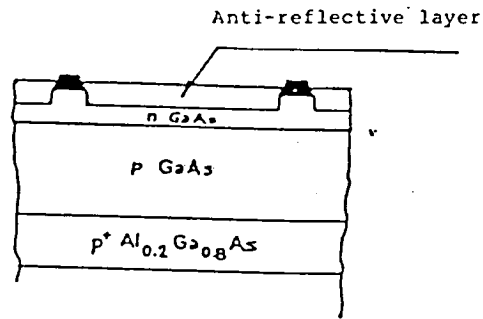


FIG. 14 SECTION DIAGRAM OF A CELL WITH A BSF JUNCTION

The voltage-current curve of the cell can be seen in Figure 15.

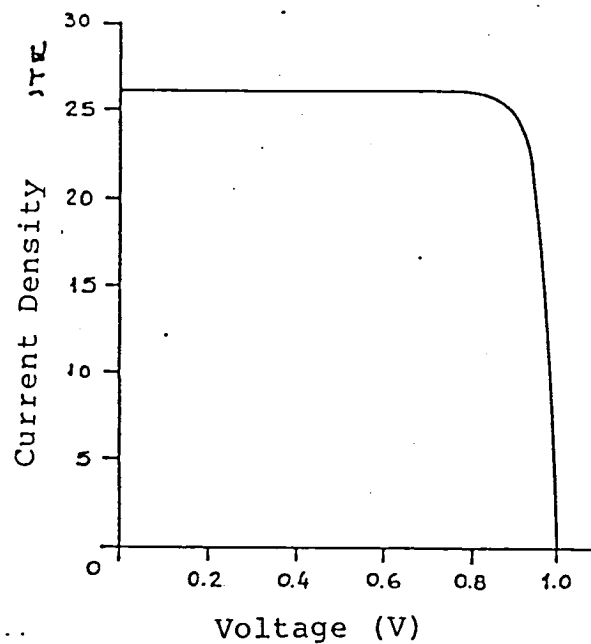


FIG. 15 CHARACTERISTIC CURVE OF A CELL WITH A BSF JUNCTION.

The resulting maximum efficiency was 22.2%, taking into account losses of surface area through the current collectors. The net efficiency of the material is 23.1%. Additional improvements are expected, so that an efficiency of 25% can be attained.

INTRODUCTION

Up to this time, propulsion of aircraft by means of solar energy (through direct conversion using photovoltaic cells) has been achieved only in very small models.

The first flight of a solar aircraft took place in 1974. The model, named SUNRISE II, was an unmanned, radio-controlled aircraft. A flight altitude higher than 5 km was attained. The Sunrise II was designed by Robert J. Boucher of AstroFlight, Inc.

In the years following, Aero Vironment Inc. undertook a project of greater magnitude. The final objective was to obtain a manned (but not radio-controlled) aircraft propelled by solar energy with the capability of flying great distances. The program was organized in two stages. In the first stage, an already existing aircraft (Gossamer Albatross II) was adapted for flight using solar energy. (The Gossamer line was designed for flight propelled solely by human energy and therefore, these were very slow models and very efficient for the weight and aerodynamics for which they were meant.) The resulting model, named the Gossamer Penguin, is in reality a version of the Albatross II on a 3/4 scale. The first flights of the model took place on April 7, 1980. At this time the solar cells were not yet attached and the motor was battery powered. The test flights using solar energy took place in July and August of the same year.

The second stage of Aero Vironment's solar program was the design of a new aircraft, with the objective of insuring its reliability in long distance flights, in normal atmospheric conditions with little turbulence. The model was called SOLAR CHALLENGER. The first flights took place at the end of 1980, and on July 7, 1981 the aircraft completed the crossing of the English Channel from France to England, marking an important milestone in the development of solar energy applied to aerodynamics.

According to the designers of the Solar Challenger (Paul MacCready, P.B. Lissaman, W.R. Morgan), the objective of the project was to demonstrate that flight is possible through the direct and exclusive use of solar energy, and at the same time to show evidence of the potential of photovoltaic energy.

GOSSAMER PENGUIN

/26

This aircraft is an ultralight model designed for a one-man crew. Its power source consists of a continuous current motor ("Astro 40"), of 12,500 rpm. The reduction case is

composed of two belt stages giving a transmission ratio of 27:1, and one chain reduction stage with a ratio of 5.17:1. The total reduction is approximately 140:1. For the initial flights, the energy was supplied by a battery composed of 28 nickel-cadmium cells, whose total weight was 3.6 kg. When the solar energy flights were begun, a panel with 3,920 solar cells (2,240 cells 2 cm x 4 cm, 700 cells 2 cm x 6 cm, and 980 cells 2.4 cm x 6.2 cm) was attached. The resulting net surface area of solar cells is therefore 4.09024 m². Under the conditions that Air Mass (AM) = 1, (which is equivalent to a clean atmosphere with low turbulence and solar radiation with normal incidence), and 1 kW/m² of incident power, the panel produced 541 W (approximately 0.73 HP). This equals an efficiency of 13.23%. Several cells were manufactured and tested by Spectrolab, Inc. and the rest were supplied by NASA.

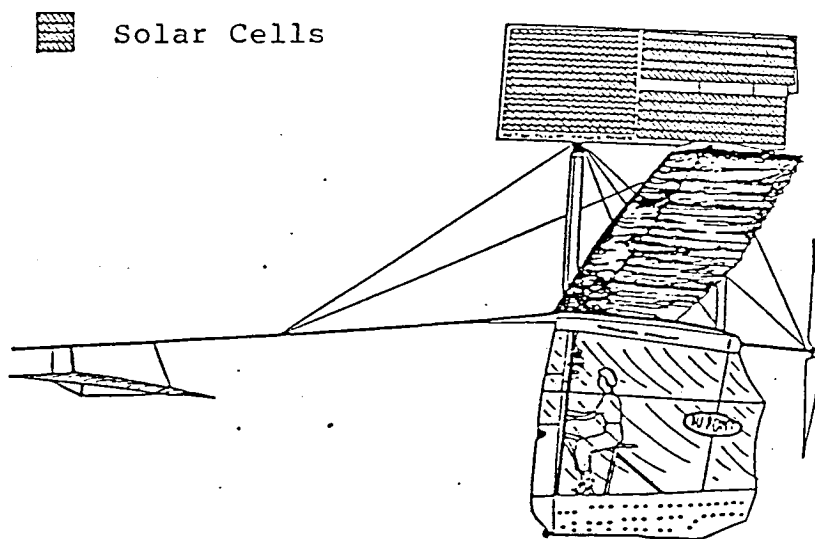


FIG. 16 GOSSAMER PENGUIN

The panel, divided into four independently connected subpanels, was placed vertically. Since the power supplied was so small that the aircraft could only be flown under very calm atmospheric conditions and with a very low sun in order to obtain an approximately normal incidence, the flights were limited to the north-south direction.

The weight of the Penguin without the panel is 23.5 kg; /27 the weight of the panel with its support structure is 7.3 kg. The weight of the empty aircraft is therefore 30.8 kg.

The wing surface area is 27.6 m², and that of the stabilizer, located at 5.5 m in front of the main wing, is 3.25 m² (canard type).

One of the fundamental problems in the development of the aircraft was the compatibility of the power curve of the motor with that of the solar cells in order to achieve their maximum utilization, simultaneously maintaining the efficiency of the propeller. The optimum transmission ratio and propeller pitch resulted from this study.

The flight speed proved to be very slow (approximately 23.5 km/h).

The chart below gives data on the original model (Gossamer Albatross II) and the model adapted for solar energy (Gossamer Penguin):

	<u>Gossamer Albatross II</u>	<u>Gossamer Penguin</u>
Empty weight	33.7	30.8
Wingspan	29.3	21.9
Surface loading (kg/m ²)	2.06	2.45
Cruising speed at sea level (km/h)	19.4	23.8
Minimum power required for the propellers (W)	190	220

TESTING AND CONCLUSIONS (GOSSAMER PENGUIN)

Low-altitude flights were attained under the best atmospheric conditions with a totally optimized system, however the aircraft was operating under limited conditions with reference to flight stability and maintenance. Nevertheless, the objective of adapting an already existing aircraft to operate by means of solar energy was realized. Following are the final conclusions which were reached based on tests of the Gossamer Penguin:

a) A variable pitch propeller is essential for obtaining a practical solar aircraft with acceptable efficiency.

b) The stability and maneuverability of the Gossamer Penguin is so improved that it cannot be the starting point for the design of heavier and faster models. /28

c). Special care must be taken in the junctions between cells, since warping caused by thermal expansion can occur.

d). Acrylic-based adhesives are appropriate for attaching the cells to a surface of a material such as Mylar, for

example, which is excellent for covering wing surfaces since it is very light and aerodynamically clean.

e). Special care must be taken in the design of the shock absorber for the landing gear in order to avoid breaking the solar cells.

f). The aircraft to be designed must have a sufficient power margin to resist descending gusts at low flight levels (for example, in the process of landing).

g). Motor cooling problems may occur in low velocity (and lightweight) models.

h). Warming of the solar cells produces a decrease in the power supplied, and this must be taken into account upon achieving the available power forecasted, especially for flights at high altitude.

SOLAR CHALLENGER

/29

1.) GENERAL CHARACTERISTICS - AERODYNAMICS

This model has a wingspan of 14.3 m, with elevated wings, without struts. Its design load is equivalent to 6 g. It is equipped with a variable pitch propeller and all the common controls of a small aircraft.

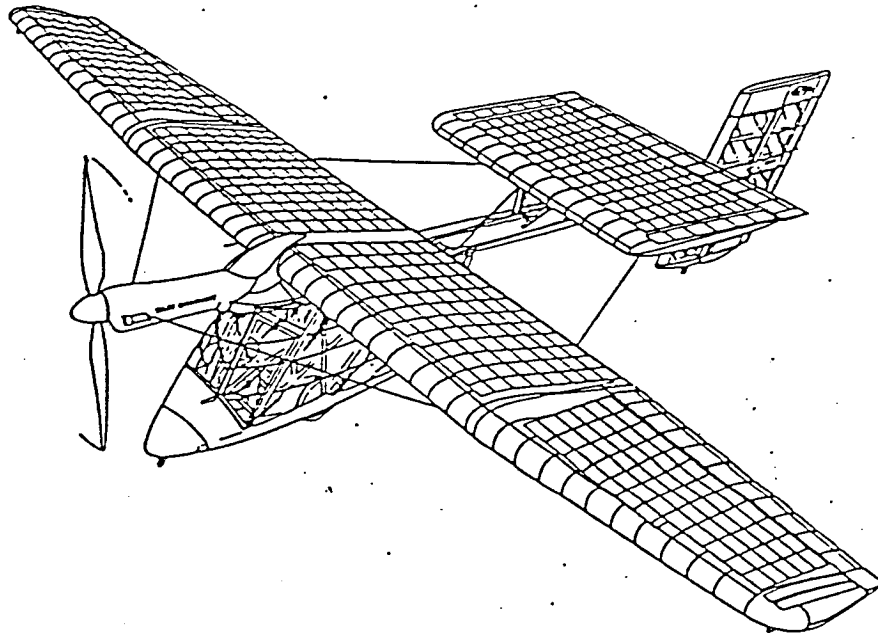


FIG. 17 SOLAR CHALLENGER

It weighs approximately 90 kg. Its unusual appearance is due to the stabilizer which is relatively large, and to the wing area, necessary to obtain the 21.9 m² required for solar cells. The propeller also turned out to be comparatively large for the efficiency requirements which were estimated at 86% for low velocities.

A study of the most effective areas in which to locate the solar cells in order to avoid shadows falling over them resulted in the following decisions:

- 1) Use of an elevated wing.
- 2) Use of a horizontal stabilizer in an elevated position.
- 3) A vertical stabilizer behind the horizontal one having the shape of a rhombus (a distorted rectangle).

Because the wing has no struts, tension wires were placed on the support surface of the wing in order to avoid bending, since this could produce warpage in the leakage edge, and eventually could cause the cells to break.

The aerodynamics of the Solar Challenger is /30 relatively conventional. However, certain practical aspects required several innovations. Since a large part of the upper surface of the wing would carry the solar cells, it was necessary to develop an aerofoil profile such that the extrados would be as level as possible. For this purpose a profile was obtained such that the extrados is perfectly straight in a span equivalent to 85% of the cord, maintaining a turbulent flow adhered to the profile for $C_l = 1$. The profile was called the Lissaman-Hibbs 8025. Tests conducted in a wind tunnel resulted in $C_{lmax} = 1.4$ with a mild stall.

A profile with a level outer section was also developed for the stabilizer, with a laminar flow in the inner section for $C_l = 0$. This profile was called the Lissaman-Hibbs 8230 and the tests confirmed the objectives of its design.

The elevators and rudders were basically sized for comparison with other already existing models of similar dimensions. The size of the ailerons was the result of a compromised solution between the necessity of producing moment of rolling and the surface area required by the solar cells, since the ailerons did not carry any cells as they are not important structural elements.

Only studies of static stability were completed, since /31 it was not considered necessary to complete calculations of dynamic stability once a model of conventional proportions resulted.

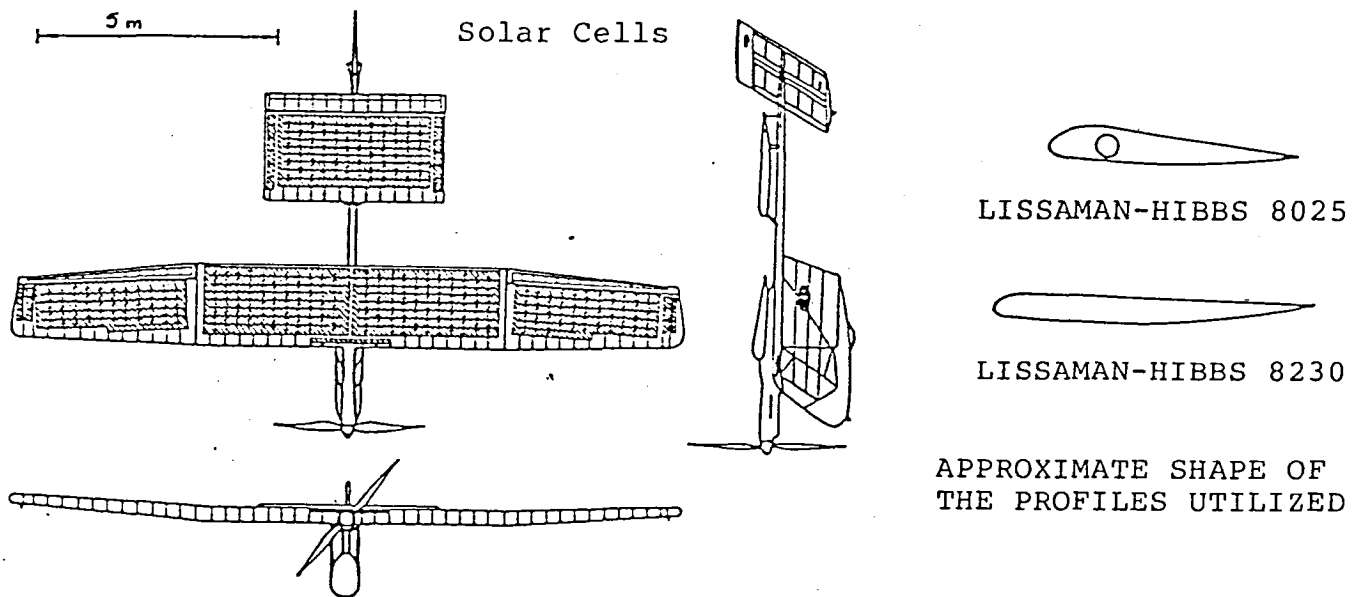


FIG. 18 THREE VIEWS OF THE SOLAR CHALLENGER

The design of the propeller was based on the theory of optimum load, as applied to the design of the propeller of the Gossamer Albatross and Penguin. The profile adopted for the blades was the Eppler 193.

2.) POWER EQUIPMENT

The power equipment consists of two continuous current motors connected to the same axle (in tandem). Each motor is run by a permanent cobalt magnet. The armature is that of an Astor motor 2500 rewound with fewer revolutions of thicker wire. The cooling and brush system was improved with respect to the original motor.

The nominal operating condition of the motor is 7,000 rpm. The reduction is in two stages. The first stage is achieved by belts at a ratio of 4.5 to 1. The second stage is by chains (cog belts) and is reduced from 5.17 to 1. Therefore the normal operating condition of the propeller is at 300 rpm.

3.) ENERGY SUPPLY

The energy is supplied by 16,128 rectangular silicon cells (with a thickness of 300 microns). These are connected in rows of up to 144 cells in series by 3 parallel rows. This parallel connection of individual cells insures the operation of the series of 144 cells even in the event of their failure or breakage, guaranteeing sufficiently reliable operation. The system connected in this manner produces a nominal voltage of 66 V, where this value depends on the temperature of the cells.

The modules of 144 x 3 cells were connected in parallel to form 5 panels, of which two were placed in each semi-wing, and the remainder in the stabilizer. Each panel is independent of the others. Within the panels, the 144 x 3 modules are connected to the principal conductor of the panel by means of a diode in order to protect the rest of the modules if one of them should short-circuit. Each panel is protected by a 10 A fuse, and may be connected to the motor one at a time. This is convenient for limiting the start-up current of the motor /32 and for modifying the power supplied in the process of descent and taxiing. During flight the 5 panels are normally connected and the power is regulated by varying the pitch of the propeller.

The instrument panel includes a power meter connected to the front motor, a speedometer and two ammeters, (one for each motor). The pitch of the propeller is determined by discerning the maximum power supplied by the front motor, and the ammeters indicate the relative distribution of power in the two motors. (Only one power meter is sufficient, since the two motors have the same characteristics).

4.) STRUCTURE

In contrast to the Gossamer Penguin, the Solar Challenger must fly dependably at high altitude and under conditions of normal turbulence. The aircraft was designed to increase safety as much as possible, even at the cost of increasing the final weight. In all the critical areas from the point of view of safety of the pilot (control and flight areas) the design criteria were conservative. The propulsion system, fuselage landing gear and instrumentation were not considered critical, and were designed with major emphasis on reducing weight. This could be done because the Challenger has the capability of landing like a glider, which is necessary in the event of failure in the propulsion system or sudden worsening of the weather conditions.

The design loads for the principal structure were +6 g; -4 g; with a safety coefficient of 1.5 and 3 for the control areas.

The fuselage was designed to support loads of +4.5 g in a vertical direction and +1 g in a transverse direction during landing, and a final load of 9.0 g (in case of collision against the ground with the aircraft flying forward and down).

Compound materials (graphite and kevlar fibers) were utilized in the primary structure. In those areas where mechanical resistance is not critical, lighter and more malleable materials such as Mylar were used, as for example in the control and flight areas, since Mylar is an aerodynamically clean substance.

The most important structural element is without a /33
doubt the principal wing spar. It consists of a tube with an
internal diameter of 178 mm. Its walls are formed by multiple
layers of graphite fibers directed at +45°. to resist
torsional and longitudinal stresses, prevent bending. This
tube is stabilized by a honeycomb of Nomex (to prevent warping
of the walls of the tube) and finally, the whole assembly is
surrounded by kevlar. This material is glued to the tube with
an epoxy resin, and its function is to prevent the rupture of
the tube, even after a breakdown, due to its great ductility.
Its total weight is 13.6 kg.

Fiberglass, polystyrene foam and sandwich panels were used
on the leakage and leading edges.

Shock absorption in the landing gear is resolved by the
use of two horizontal nylon beams (having a low unit of
elasticity) which absorb normal loads from smooth landings and
taxiing, and a Kevlar pseudo-spring which absorbs additional
shock in the case of an rough landing.

Testing of the wing took place using loads equivalent to
84% of the design load, with satisfactory results. The rest of
the structure was successfully tested up to 100% of the design
load.

5.) THE CROSSING OF THE ENGLISH CHANNEL

After about 50 test flight hours, evaluations were made
and certain minor modifications were incorporated. New
instruments (a directional gyro and new radio equipment) were
added to the already existing instruments (speedometer,
compass, variometer, and motor instruments), plus 2 additional
modules of 60 solar cells to supply energy to the new
instruments, and a battery for emergency use, capable of
providing 30 minutes of flight without the supply of energy
from the cells. The final empty weight was 98.6 kg.

On July 7, 1981 the crossing of the English Channel took
place, from the airport of Pontoise-Cormeilles to the Manston
Base of the Royal Air Force, covering a distance in a straight
path of 262 km. The flight lasted 5 hours and 23 minutes, the
maximum altitude reached was 3500 m, and the maximum true air
speed was 70 km/h.

6.) PERFORMANCE

/34

Since the fundamental objective of the Aero Vironment
program was to complete the France-Great Britain flight, it was
not possible to complete an exhaustive study on the energy and
performance capabilities. In any case, specific results were
obtained.

The power consumed while cruising at an altitude of 3.3 km

was 2500 W (3.35 HP). During initial ascent power consumption was 2800 W. These values determine an approximate yield by the cells of 11.6%. It is estimated that in optimum isolation conditions at sea level, 2550 W can be obtained, and at an altitude of 15 km, 4100 W (5.5 HP) can be obtained.

The motor efficiency was calculated at 78%, the reduction efficiency (by belt and cog belt) was calculated at 95%, and that of the propeller at 85%.

The aircraft requires a minimum of 1400 W (1.9 HP) to maintain horizontal flight in a completely calm atmosphere.

The maximum ratio C_L/C_D was calculated at 15.7, which corresponds to a flight velocity of 42.5 km/h.

The following figures indicate estimated performances of the Solar Challenger:

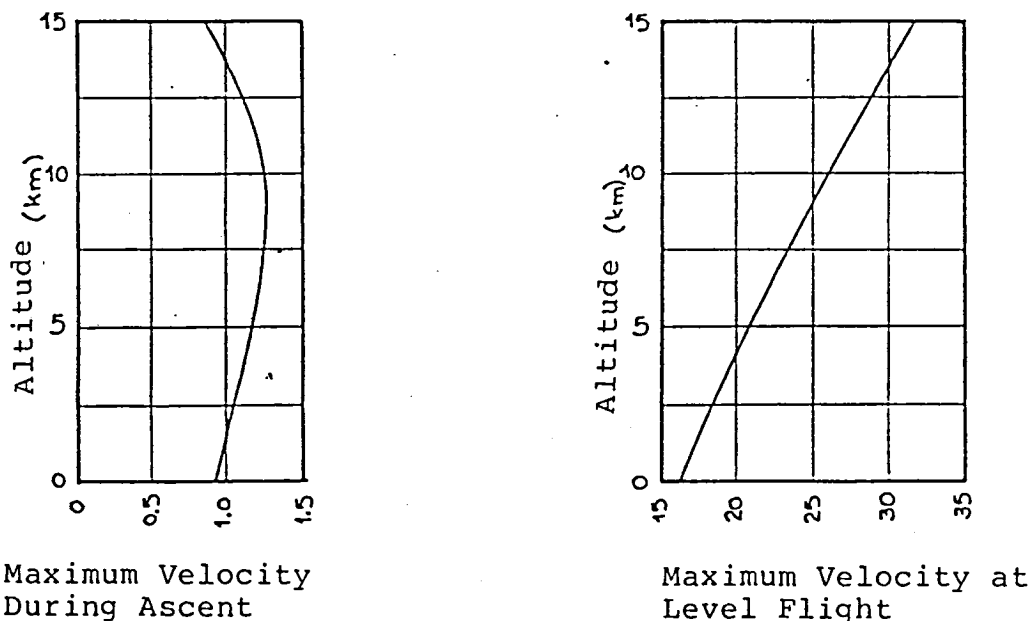


FIG. 19 PERFORMANCE OF THE SOLAR CHALLENGER AS A FUNCTION OF FLIGHT LEVEL.

7.) ADDITIONAL OBSERVATIONS

/35

a). It was observed that the presence of clouds did not weaken the energy received by the cells as it had been originally assumed. As long as the sun is not blocked, the dispersed energy can reinforce the direct energy, increasing the amount of energy received by more than the standard value corresponding to AM = 1.

b). In order to calculate the performance of a certain

aircraft in a particular flight mode, the orientation of the cells relative to the sun is a critical factor to remember, in order to determine the rest of the parameters to be calculated.

SOLAR HAPP

/36

1.) INTRODUCTION

HAPP is the abbreviation for High-Altitude Powered Platform. The project for this solar aircraft is being completed by Lockheed Missiles and Space Company, under contract with NASA Langley Research Center. From certain preliminary studies on propulsion systems and structures made in 1982-83 regarding the adaptability of this project, a prototype of this aircraft was completed, and its /36 versatility for agricultural missions, particularly over Phoenix-Tucson-Tombstone (Arizona) was analyzed. If the project goes forward, it is hoped that the first flight of the aircraft will take place in 1993.

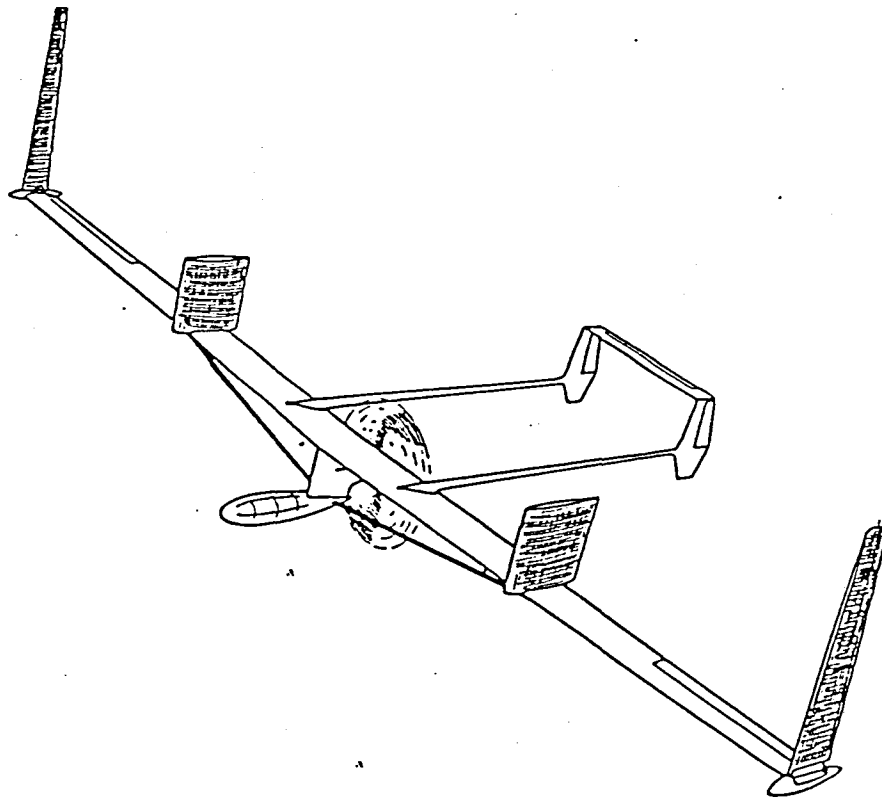

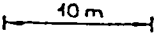
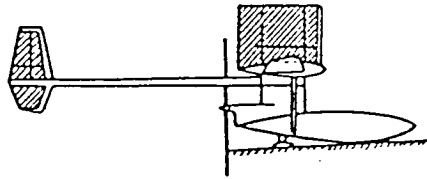


FIG. 20 SOLAR HAPP. FLIGHT IN DAYTIME CONFIGURATION

 Solar Cells
 10m



/37

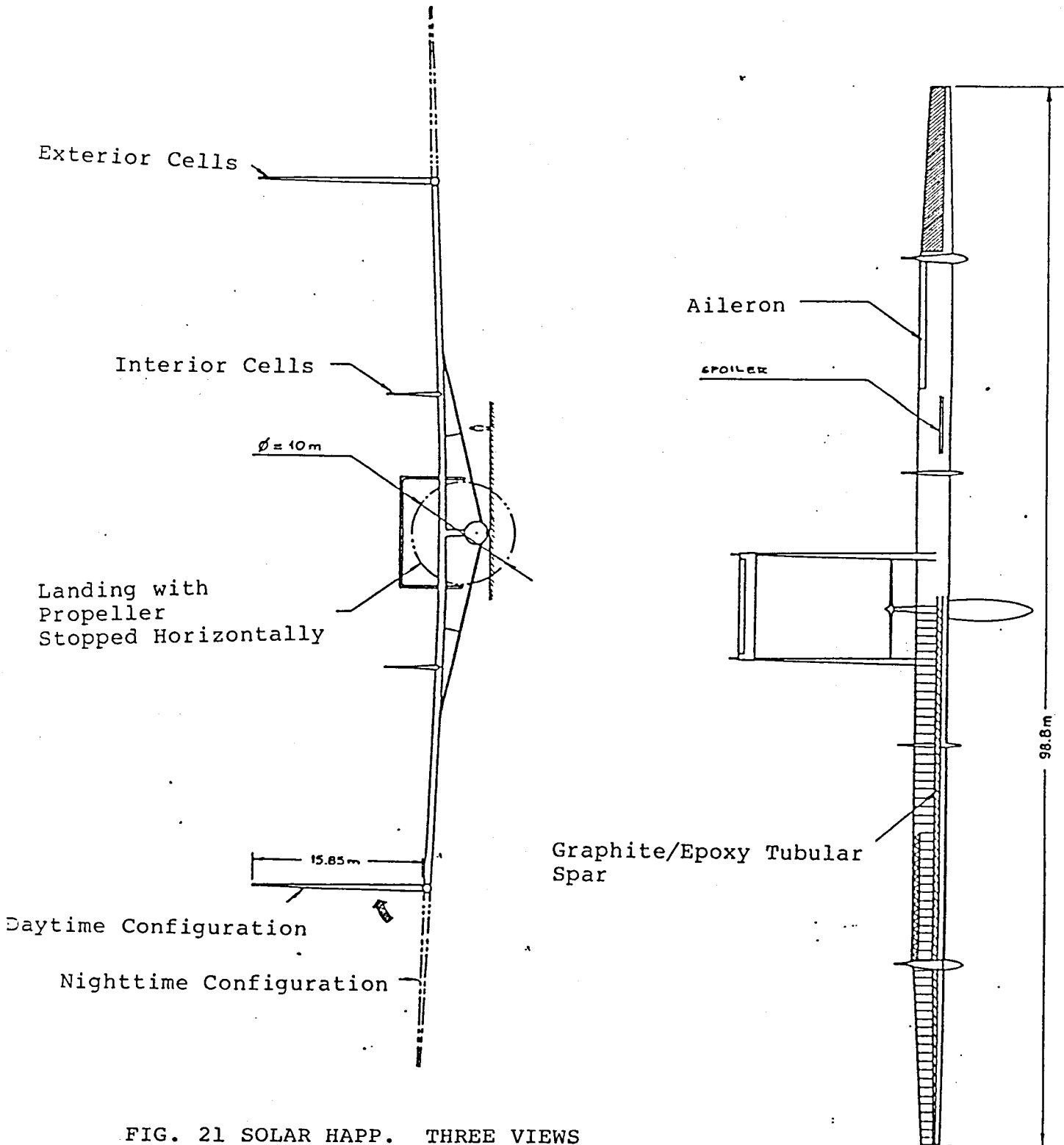


FIG. 21 SOLAR HAPP. THREE VIEWS

The aircraft was designed for radio-controlled flight at an altitude of 20 km for a one year period, carrying a useful load of 110 kg. Figure 21 shows three views of this aircraft.

The systems on board are:

- a) Energy collector and storage system.
- b) Rotating components (motor, gearbox and propeller).
- c) Automatic pilot and flight controls.
- d) Navigation system.
- e) Useful load.

The wingspan will be 98.8 meters, and the length, 28 meters. The total weight is estimated at 910 kg, of which 110 kg will be useful load. The wing area is 281 m², creating a wing load of 3.24 kg/m². This value is extremely low, especially compared with the wing load of a passenger aircraft (500 kg/m²), a light aircraft (50 kg/m²) or an aerodynamic model (4 kg/m²).

The most critical element of the aircraft is the principle spar. This will be constructed of a tube of graphite fiber and epoxy resin, using a solution similar to that utilized by the Solar Challenger.

The wing tips will be mobile. During daytime flights, they will be in a vertical position to take better advantage of the solar light. During the night the wings will adopt the horizontal position (see Figure 21) to improve the aerodynamic characteristics of the model. Both the inner and the outer surfaces of the wing tips will be covered by solar cells. Vertical surfaces will be placed on the wing 12.5 meters from the center of the wing on both sides. The area of each of these surfaces will be 24.5 m². These surfaces will also carry solar cells on both of their sides. The vertical tail unit will also be covered by cells. The total surface area covered by cells will be approximately 276 m².

The planned aircraft will have the following characteristics:

Cruise velocity	96 km/h
Altitude	20 km
Power consumption	13 HP

<u>Gliding Ratio</u>	
Daytime configuration	24:1
Nighttime configuration	30:1
Speed loss at sea level (Nighttime configuration)	20 km/h
<u>Maneuverability:</u>	
Minimum rotation radius	495 m
Inclination	3.7°
<u>Landing:</u>	
Angle of descent	1.9°
Taxiing to a stop	18 meters

3.) PROPULSION AND ENERGY SYSTEM

This is the most important system of the aircraft. It is composed of the solar cells, the energy storage system and the motor system. The excess electrical energy supplied by the solar cells will be stored through the production of chemical compounds, specifically hydrogen and oxygen, from electrolysis of a specific water mass. Therefore, the system will consist of the electrolysis tank and the combustion cell where the stored energy will be recovered. An energy distributor (connected with the solar cells, the electrolysis tank and the combustion cell) will feed the motor. It will also supply energy to the navigation systems, to the automatic pilot, the flight controls and to the useful load sensors. Figure 22 shows a diagram of the complete system.

By day the motor will be fed directly by the cells, and ^{/40} the excess energy will be stored. At nightfall, the motor will operate by means of the combustion cell.

At cruise altitude, the maximum efficiency of the cells will be 14.5%. The quantity of energy transmitted to the aircraft will have a lower yield, since it will be affected by the following efficiencies:

Energy distributor	0.92
Electrolysis tank	
Storage of reactants	0.56
Combustion cell	
Motor - Reduction case	0.87
Propeller	0.86
This results in final yield of only	5.6%

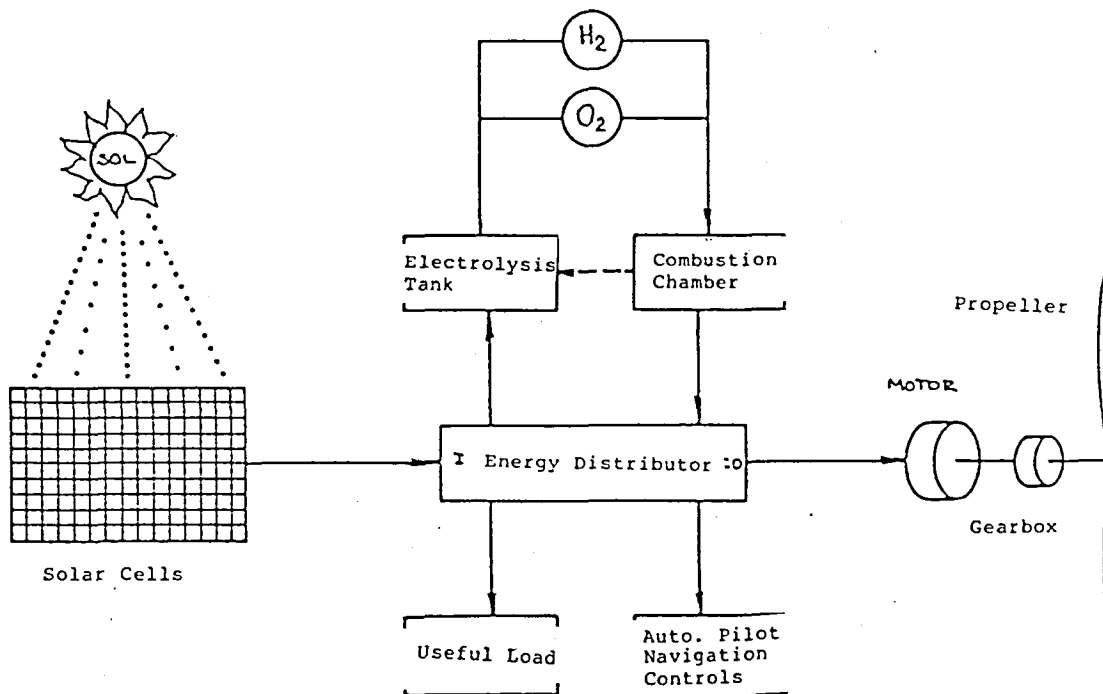


FIG. 22 SYSTEMS OF THE SOLAR HAPP

4.) COMMUNICATION AND ENERGY DISTRIBUTION SYSTEMS

The systems which require the supply of energy, in addition to the propulsion system, are the automatic pilot, the flight controls, the navigation system and the useful load sensors. Navigation will be accomplished using satellites of the Global Positioning System (GPS). The GPS receptor is the aircraft's primary communication medium. It will have two transmitter-⁴¹ receivers to communicate with the earth station; one to control the automatic pilot and the flight control systems, and another to receive information from the sensors which compose the useful load. For reasons of weight, only indispensable information will be processed on board. Since the aircraft will be in permanent contact with the Earth station, only the information obtained by telemetry will be processed.

Figure 23 shows a diagram of the communication and energy distribution systems.

5.) OPERATIONS

Takeoff and Ascent

Takeoff will take place at night, under calm wind conditions. The aircraft will be placed on a rolling platform, and will be joined to the tow truck with a cable. The truck will pull the aircraft on the platform until reaching takeoff

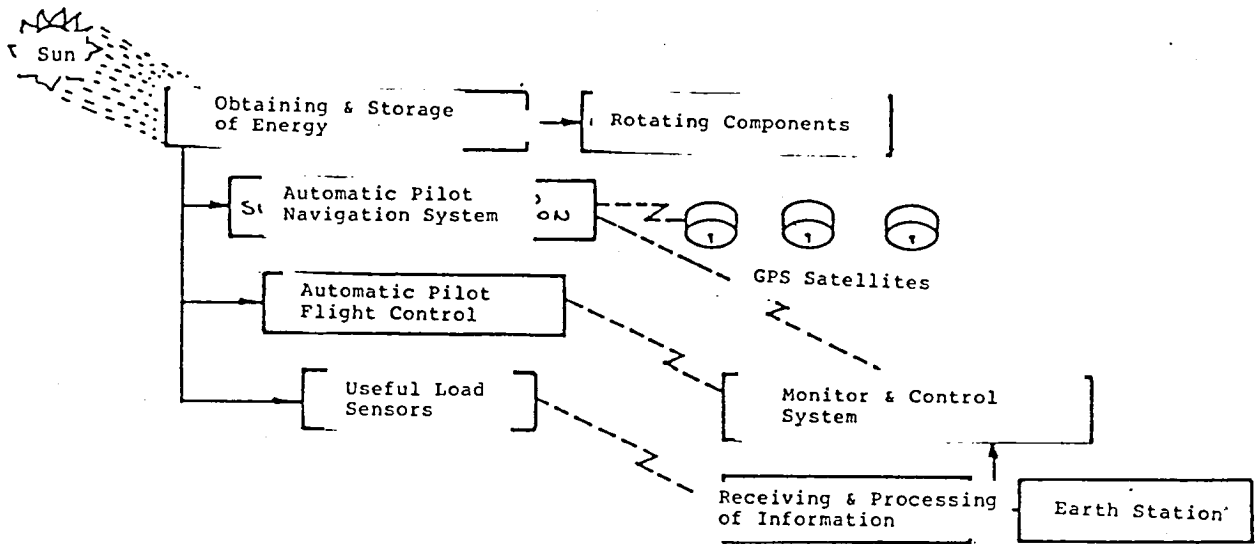


FIG. 23 DIAGRAM OF THE COMMUNICATION SYSTEM OF THE SOLAR HAPP

speed. At this moment the aircraft will leave the platform and gain altitude. At 21 meters the aircraft motor will start, and when the propeller drive has stabilized, the tow cable will come unfastened. The complete operation will last approximately one minute.

Ascent

Ascent to the altitude of 20 km will take 3 hours.

Descent and Landing

/42

The maximum landing speed permitted is 18.3 km/h, which signifies that in little more than an hour the aircraft will have reached sea level (from the cruise altitude). When visual contact has been made between the aircraft and the earth station, the final gliding angle of 1.9° will be established. At an altitude of 30 meters, the propeller will be stopped in a horizontal position and feathered.

6.) POSSIBLE FAILURES AND DIFFICULTIES

The very particular aerodynamic configuration of this aircraft (aeroelastic and structural) creates new difficulties which must be noted. The low wing load makes the model very sensitive to the predominate meteorological conditions, especially to gusts and turbulence. Given the relatively large moment of inertia, the aircraft's response to controls will be slow. This implies that the automatic control systems must be very fast and effective.

If the aircraft is naturally stable according to its three

principal axes, it is not stable in the spiral mode. Therefore, rotations must be made very slowly and with a small bank angle.

Another fundamental aspect to be noted is flutter, since this aircraft has very particular aeroelastic properties because of its large wingspan and low structural rigidity.

7.) USEFUL LOAD

Information will be obtained according to 7 spectral bands.

<u>Wavelength</u>	<u>Characteristic</u>	<u>Detection</u>	<u>/43</u>
4500 to 5200	Visible - blue	Air and water pollution	
5200 to 6000	Visible - green	Air and water pollution	
6300 to 6800	Visible - red	Absorption of Chlorophyll	
7600 to 8000	IR near		
15500 to 17500	IR medium		
20500 to 23000	IR medium		
105000 to 235000	IR distant	Vegetal stress	

INTRODUCTION

The flight of the Solar Challenger showed that it is possible to fly with solar propulsion exclusively. At the end of their work, the designers reached the conclusion that the design of a radio-controlled aircraft propelled by solar energy is feasible. This concept was studied by Lockheed Missiles & Space Co. in 1982-83 in a study requested by NASA Langley Research Center. The study continued in 1984-85, resulting in the prototype of the Solar HAPP and a preliminary analysis of an agricultural mission.

The simple fact that NASA and Lockheed are interested in a solar aircraft project indicates that the degree of feasibility is high.

However, it must be noted that both the Solar Challenger and the Solar HAPP are very unusual aircraft. In both cases, the available power is small, requiring innovative solutions regarding structure, material, and aerodynamics. The work is being done under conditions that allow very little margin. Both projects tried to achieve drastic reductions in resistance and weight to be able to utilize the available energy successfully.

We must add the high cost and low efficiency of the solar cells to all of the above. There exists a physical limit of availability, since 930-1100 W affect, at most, one square meter of cells. Although the difficulties to be surmounted are many and very important, we cannot eliminate this system of propulsion. Advances in aeronautics have been so significant since December 17 of 1903, when the Wright brothers completed the first successful flight of an aircraft, that today nothing seems impossible.

Propulsion exclusively by solar energy is not the only answer. Other solutions using new concepts may have successful results. One of these might be the use of hybrid motors.

SOLAR REACTION MOTOR

/46

Turboreactors currently possess the following devices: diffuser, compressor, combustion chamber, turbine, and nozzle. The power required by the compressor is supplied by the turbine, however, the turbine is the critical element of the motor, since it works at high temperature and under strong mechanical stress. This limits the maximum temperature of the fluid at the outlet of the combustion chamber to limiting values of 1200°C (cooling blades). Appendix 3 shows that the maximum temperature notably influences improvement in the yield

of the Joule-Brayton cycle (with losses).

A motor which accomplishes the same cycle without high temperature restriction would be very desirable. However, if the turbine stages are eliminated, the compressor must be fed by an external source. The compressor could be driven by solar energy through an electric motor. The basic problem is that there is limited energy from that source. (A Boeing 737 with approximately 77 m² of wing area, having solar cells with an efficiency of 25%, would only produce 26 HP). Additional modifications to the motor are necessary in order to effectively utilize such low power.

Low power in the compressor implies a low compression ratio. Since the efficiency of the simple Joule-Brayton cycle depends fundamentally on the compression ratio (see APPENDIX 3) it is obvious that its use would not be effective.

Appendix 3 describes a study of the Joule-Brayton cycles, especially the variables which affect efficiency. The following is based on Appendix 3.

If the compression ratio is low, the only possibility is to utilize the regenerative cycle. According to calculations, thermodynamic efficiency is sufficiently high at approximately 60%. The degree of regeneration is the most important subject in this case.

The proposed motor would have the following systems: diffuser, compressor (electric motor), combustion chamber, nozzle, regenerator. Nevertheless, this motor has various problems which must be resolved. First we will discuss the advantages.

With the elimination of the turbine, the critical 47 elements are now the combustion chamber and the regenerator nozzle. These components will operate at very high temperatures (1950 to 2000°C), but with low mechanical stress. This would allow the partial or total use of ceramic materials. The Motoren un Turbinen Union Company (MTU) of Germany conducted advanced research on the use of ceramic materials in conventional turboreactors reaching temperatures of 2000°C. The ceramic components were manufactured at reasonable cost using nitride and silicon carbide as the basic ingredients. The addition of boron or beryllium nitride notably improves the tenacity of the material. Again, the resistance of the material will set the physical limits of temperature, but given the absence of great stress, this occurs at higher temperature.

Though the addition of the regenerative device might increase the weight of the unit, there could be one favorable compensation for the elimination of the turbine. The weight of the electric motor is compensated by the smaller size of the compressor.

Now we will examine the difficulties.

The lower the compression ratio, the higher the regeneration efficiency required. The optimum solution for the three variables--compressor power, compression ratio, and regeneration efficiency--must be found.

The critical mode for this motor would be that of takeoff. Since there is no spontaneous air flow, because the aircraft is not moving, all the compression must originate from the compressor, without the assistance of the inlet diffuser. If a motor can be constructed which would give the necessary thrust for takeoff, the ascent or cruising modes would be feasible with complete safety. It is very probable that an energy storage unit may be necessary to be able to provide more power to the compressor on takeoff. In addition, there must be enough energy reserves to complete a landing in the event of bad weather. This might add excessive weight to the unit. The storage system could recharge itself during cruise flight, since the diffuser could eventually operate without the total support of the compressor. The estimated calculations gave promising results, though these must be carefully verified. Figure 24 shows a diagram of the proposed motor.

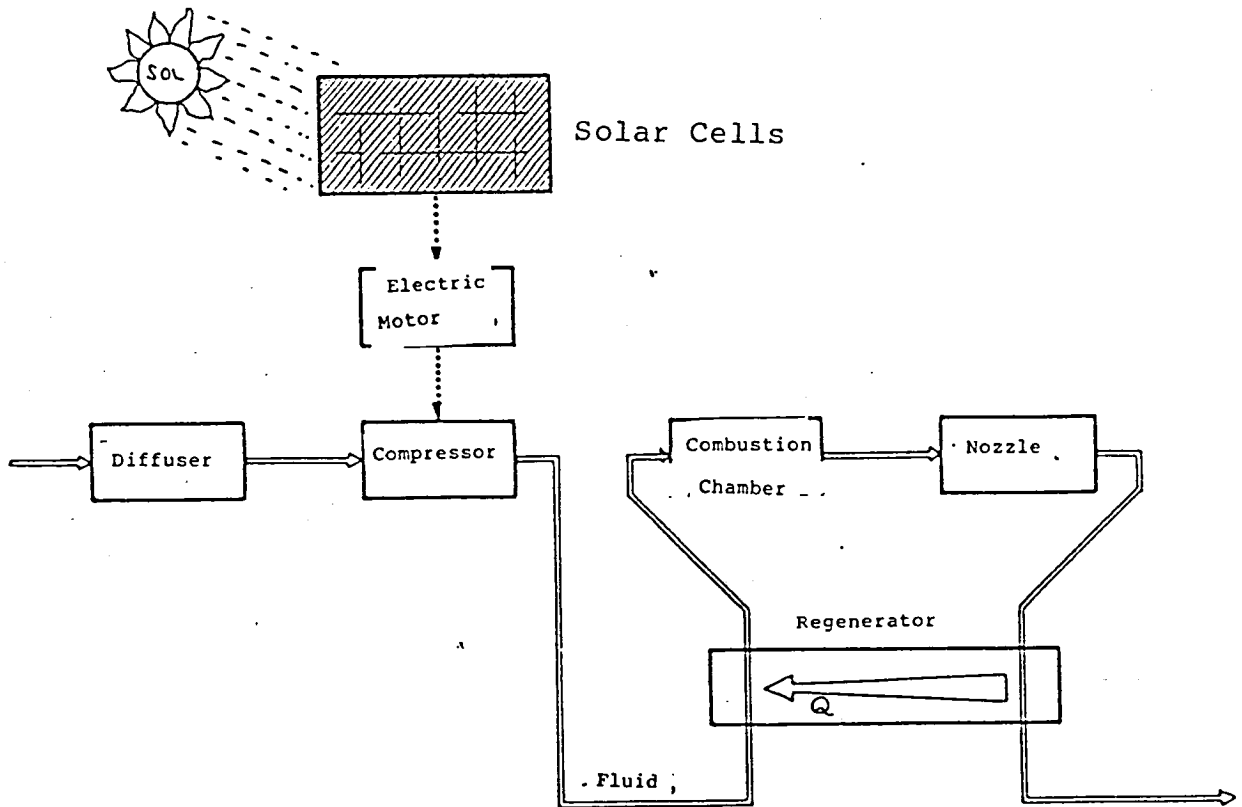


FIG. 24 (See also Figure R - Appendix 3)

Taking the particular case calculated in Appendix 3 as /48
an example, the following can be noted: In the event that
there is no regeneration, the air-fuel ratio is 16.6. The
theoretical ratio is 15. The excess air coefficient is
therefore 1.1. However, with a regeneration of 75%, the air-
fuel ratio increases to 47.6. The excess air coefficient also
increased, to 3.2. This signifies that varying the amount of
fuel can increase the high temperature even more, thereby also
increasing the thrust. Therefore, the possibilities of the
motor are increased, and in fact the material of the chamber
sets the maximum limit for temperatures.

Another problem to be considered is the loss of ducts,
since the fluid does not follow a purely axial course, since it
completes two rotations of 180°. These losses must be
minimized for the system to be economical.

ADDITIONAL COMMENTS

/49

The proposed motor is based on what could be called
"little disturbance". A small compressor frees a very powerful
process which is then almost self-maintained through the
transfer of energy in the regenerator. This means that little
external power is required to take advantage of the combustion
energy, almost without losing energy in the discharge of gases
to the atmosphere given the existence of the regenerator.

It must be noted that the system was proposed to improve
the efficiency of a reaction motor with the aid of solar
energy, but it could be used with other external energy sources
in the event that the compressor is not necessary during cruise
flight.

In summary, it must be clearly stated that the
calculations presented in Appendix 3 are only approximate,
since the necessary data was not available; therefore some
values were estimated while others were assumed. The
calculations were done with the objective of verifying orders
of magnitude; however, the proposed concept is more important
than the results obtained (which I do not consider to be
completely reliable). Physically, it seems to be a good
solution, but the technological, material, and economic aspects
remain the decisive factors.

October 8, 1985

[signed] Ladislao Benedek

APPENDICES

APPENDIX 1 - COMPTON EFFECT

/51

The concept of the photon as an energetic entity with dual performance - that is, electromagnetic and particle waves according to the physical phenomenon in which it occurs - was confirmed in 1923 by A. H. Compton, who won the Nobel prize for this work in 1927.

For example, when a group of X-ray photons with a wavelength λ fall on a graphite block, it can be observed that the dispersed X-rays are of different wavelengths showing two peaks of intensity. One of these is the same as the incident wavelength, and the other shows a greater wavelength, λ' .

Compton explained the phenomenon in the following way:

The incident photons possess energy,

$$E = h \nu \quad (h = \text{Planck constant} = 6.63 \times 10^{-34} \text{ Joule cycle})$$

Upon colliding with the free electrons in the dispersion block, the photons escape dispersed with a lesser energy, since the electrons absorbed part of it. This implies that the frequency had to decrease, since h is constant. However, if the frequency decreases, the wavelength increases, since $c = \lambda \nu$ ($c = \text{speed of light}$).

The valid equations for this case, taking relative corrections into account, are as follows:

$$m = \frac{m_0}{\sqrt{1 - \frac{v^2}{c^2}}}$$

where $m_0 = \text{mass at rest}$
 $m = \text{mass at speed } v$

$$K = mc^2 - m_0c^2$$

Where $K = \text{kinetic energy}$

$$p = mv$$

where $p = \text{quantity of movement}$

For one photon equals:

$$K = mc^2 - 0 = mc^2 = h\nu$$

$$p = mc = mc^2/c = K/c = h\nu/c$$

For an electron, instead, this equals:

/52

$$K = mc^2 - m_0c^2 = \sqrt{\frac{m_0^2 c^4}{1 - \frac{v^2}{c^2}}} - m_0c^2$$

$$K = \sqrt{\frac{m_0^2 c^2 (c^2 - v^2 + v^2)}{1 - \frac{v^2}{c^2}}} - m_0c^2$$

$$K = \sqrt{\frac{m_0^2 c^2 [c^2 (1 - v^2/c^2) + v^2]}{1 - \frac{v^2}{c^2}}} - m_0c^2$$

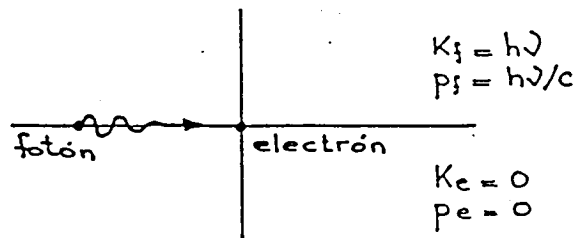
$$K = \sqrt{m_0^2 c^2 \left[c^2 + \frac{v^2}{1 - \frac{v^2}{c^2}} \right]} - m_0c^2$$

$$K = \sqrt{m_0^2 c^4 + \frac{m_0^2 v^2 c^2}{1 - \frac{v^2}{c^2}}} - m_0c^2$$

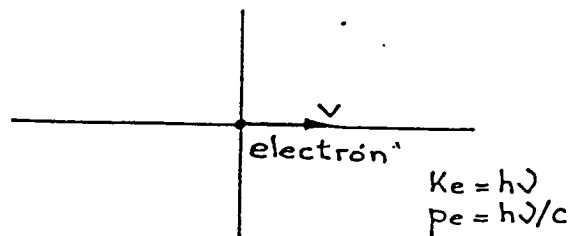
$$K = \sqrt{(m_0c^2)^2 + p^2c^2} - m_0c^2 \quad (*)$$

We will demonstrate below that the photoelectric effect is not possible with a completely free electron.

Before the absorption of the photon, we have:



After the absorption, we have:



Referring to equation (*):

$$h\nu = (m_0c^2)^2 + h^2\nu^2 - m_0c^2$$

$$h\nu + m_0c^2 = (m_0c^2)^2 + h^2\nu^2$$

$$h^2\nu^2 + 2h\nu m_0c^2 + m_0^2c^4 = m_0^2c^4 + h^2\nu^2$$

From which we obtain:

$$2h\nu m_0 c^2 = 0$$

This result is absurd, since

/53

$$h \neq 0, \nu \neq 0, m_0 \neq 0, c \neq 0$$

The result of this is that an electron cannot simultaneously absorb the TOTAL energy and the TOTAL amount of movement attracted by the photon. Therefore, the photoelectric effect cannot exist in the case of a free electron. In a collision such as that mentioned, only one part of the energy is taken by the electron, and the photon follows its path with a minor frequency. The loss of energy mentioned is one of the reasons that less solar energy is received on the earth's surface due to the presence of the atmosphere.

APPENDIX 2 - CHARACTERISTICS OF SOME SILICON SOLAR CELLS

/54

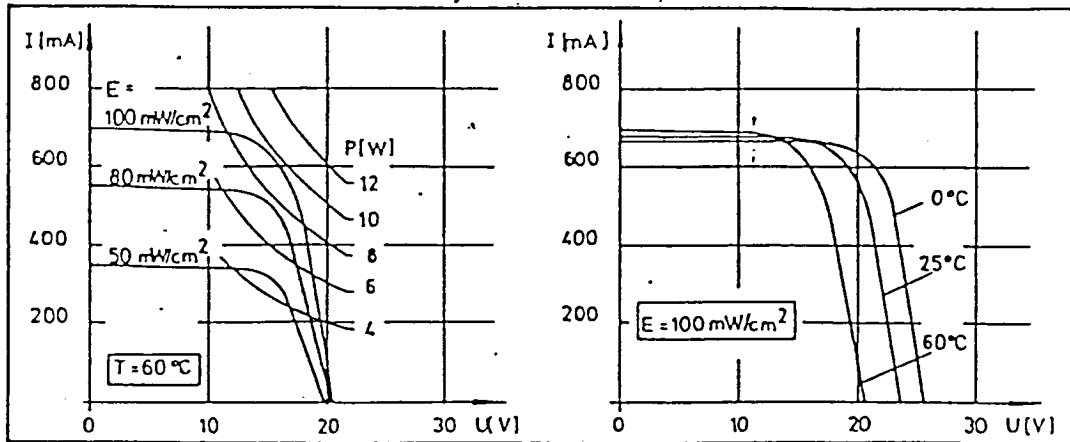
1.) AEG-TELEFUNKEN

MODULE TSG MQ 40/0

Material: monocrystalline silicon
 Specific resistance: 2 cm
 Equipment: n-p
 Cell dimension: 5 x 5 cm²
 Number of cells: 40
 Shield: crystal
 Frame: aluminum
 Weight: 1430 g
 Efficiency (25°C): 8.6%

Characteristic Variables (AM1 - 1kW/m²)

	Testing Temperature			
	-40°C	0°C	25°C	60°C
Open circuit voltage (V)	29.2	25.7	23.5	20.4
Short circuit current (mA)	669	679	685	694
Current for maximum power (mA)	614	624	630	639
Maximum power (W)	14.8	12.8	11.6	9.7
Maximum power per useful area (W/m ²)	110	95	86	72



2.) SOLAREX CORPORATION

/55

MODULE HE 60 G

Material: Monocrystalline silicon
 Equipment: n-p
 Cell dimension: 6.3 x 6 cm
 Number of cells: 72
 Shield: Crystal
 Frame: Aluminum
 Antireflectant film: Tantalum oxide
 Weight: 3.8 kg
 Efficiency (25°C): 11.6%

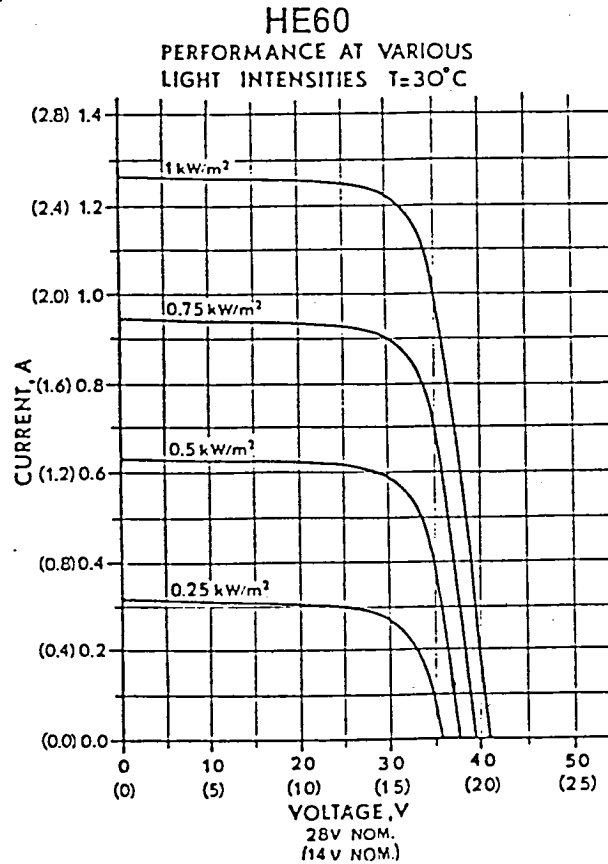
Characteristic Variables
(AM 1 - 1kW/m²)

Test Temperature
25°C -40°C

Open circuit voltage (V)	20	
Short circuit current (A)	2.56	
Current for maximum power (A)	2.31	
Maximum power (W)	37	43
Max. power per useful area	114	132

Power varies - 0.3 % /°C

Open circuit voltage varies -
 0.4 % /°C.



3.) ARCO SOLAR, INC.

/56

MODULE M51

Material: Monocrystalline silicon
 Cell dimension: 4" in diameter
 Number of cells: 35
 Shield: Glass
 Weight: 5.7 kg
 Efficiency (25°C): 10.76% (for the module)

Characteristic Variables
(AM1 - $1\text{kW}/\text{m}^2$)

Test Temperature
 25°C

Open circuit voltage (V)	21
Short circuit current (A)	2.6
Maximum power current (A)	2.31
Maximum power (W)	40
Power/area (W/m^2)	116
Power/useful area (W/m^2)	140

The net efficiency of the cell is: 14%

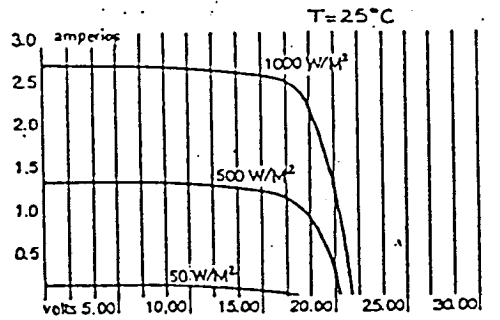
GENERAL INFORMATION - SILICON CELLS

Manufacturer	Material	Cell Size	No. of Cells	Module	Encapsulation	P _{max} (W)	η% (net)
Arco Solar Inc.	monocrystal	4" -diam.	35	ASI-16-2300	V/PVB/P/MAL	37	13
Solar Power Corp.	monocrystal	4" -diam.	36	G12-361	V/SIL/P/MAL	33	11,3
Solarex	monocrystal	6,3 x 6 cm ²	72	HE60	SIL/P/MAL	37	11,4
Motorola	monocrystal	10 x 10 cm ²	33	MSP43A40	V/PVB/P/MAI	40	12
Phtowatt	monocrystal	4" -diam.	35	41S35GC	V/SIL/V/MAL	32	11,3
Lucas	monocrystal	4" -diam.	36	M 12-361	SIL/P/FPR	31	10,6
AEG-Telefunken	polycrystal	10 x 10 cm ²	10	PQ 10/10/0	V/PVB/V/MAL	9,6	9,6

References:

V: glass
 PVB: polyvinylbutyral
 SIL: silicon
 P: polyester

MAL: aluminum frame
 MAI: stainless steel frame
 FPR: reinforced plastic fibers



APPENDIX 3 - JOULE-BRAYTON CYCLE

/58

The basic cycle used in gas turbines is that called "non-regenerative open cycle," or "Joule-Brayton cycle." Figure A shows the corresponding T-S diagram.

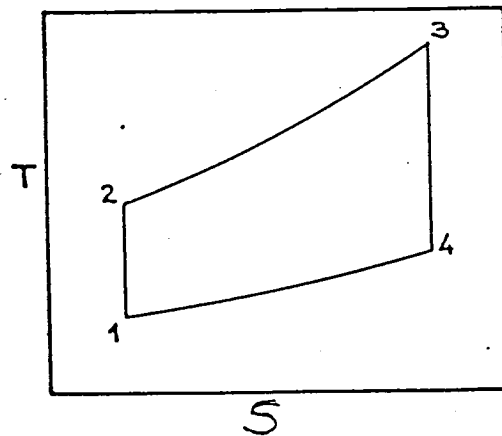


FIG. A JOULE-BRAYTON CYCLE

1.) THE IDEAL CYCLE

Following are the processes (considered reversible):

- 1-2 Compression (compressor)
- 2-3 Addition of isobaric heat (combustion chamber)
- 3-4 Expansion (turbine and/or nozzle)
- 4-1 Loss of isobaric heat (in the atmosphere)

If we consider the cycle to be ideal, then there are no losses of any kind; therefore:

$$\begin{aligned}
 S_1 &= S_2 \\
 S_3 &= S_4 \\
 P_2 &= P_3 \\
 P_4 &= P_1
 \end{aligned}$$

From the study of this cycle, in which the quantity of fuel burned in the 3-4 process is also depreciated but does not reach the 1-2 process, and assuming that the substance which travels the cycle is only air, the thermodynamic efficiency of the cycle is:

$$\eta_t = 1 - \frac{1}{\pi^m} \quad ; \quad \text{with} \quad m = \frac{k-1}{k}$$

where:

/59

π is the compression ratio, P_2/P_1
 k is the ratio of specific heats, C_p/C_v

If $k = 1.4$, then $m = 0.286$

From this we observe that

$$\eta_t = 1 - \frac{1}{\pi^{0.286}}$$

Consequently, we see that the efficiency of the ideal cycle depends solely on the compression ratio and that it is not a function of the hot temperature, T_3 . The higher the compression ratio, the higher the efficiency of the cycle.

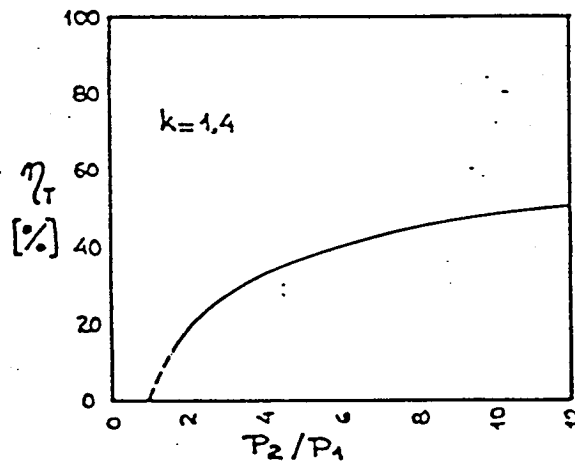


FIG. B EFFICIENCY OF THE JOULE-BRAYTON CYCLE

In order to obtain the expression of efficiency, it was assumed that the value of C_p is constant.

2.) THE REAL JOULE-BRAYTON CYCLE

Since the processes that occur in all thermodynamic evolutions are irreversible, the actual efficiency is less than the ideal. The processes of compression (1-2) and expansion (3-4) are not isoentropic unless an increase of entropy exists in them. In addition, when there is a loss of pressure in the

combustion process (2-3) and P_4 is a little greater than P_1 in the discharge to the atmosphere (4-1), the efficiency decreases even more. In Figure C, the continuous solid line represents the real cycle. The corresponding ideal cycle is represented by a dotted line.

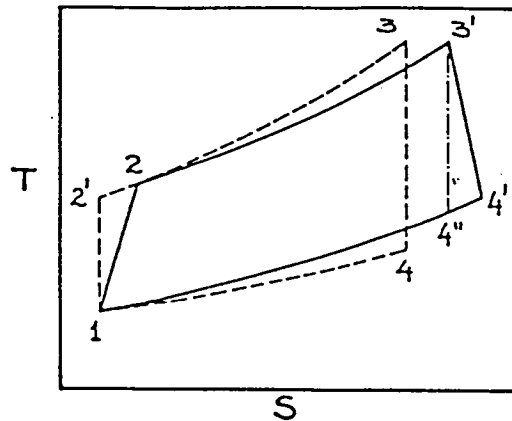


FIG. C ACTUAL JOULE-BRAYTON CYCLE

In the real cycle being considered it was assumed that /60 the compression ratio P_2/P_1 is the same as that of the ideal cycle superimposed on it, and that the hot temperature T_3 is the same for both.

The result in this case is:

$$\begin{aligned} S_1 &< S_2 \\ S_3 &< S_4 \\ P_2 &> P_3 \\ P_4 &> P_1 \end{aligned}$$

Losses, in general, are as follows:

a) COMPRESSOR. Greater power must be supplied to the compressor than that theoretically required to reach the compression desired. Its yield, which expresses the ratio between the two powers mentioned, is calculated as follows:

$$\eta_c = \frac{h_2' - h_1}{h_2 - h_1}$$

b) COMBUSTION CHAMBER. A pressure drop can be verified in the combustion chamber as well as in the front and rear ducts.

c) COMBUSTION CHAMBER. Losses due to incomplete combustion (Not all the fuel energy is used).

d) TURBINE. The load transmitted to the turbine rotor is

less than that theoretically supplied by the fluid which circulates in it. The efficiency is defined as:

$$\eta_{\tau} = \frac{h_3' - h_4'}{h_3 - h_4''}$$

e) NOZZLE Losses through non-reversibilities exist. In addition, the discharge pressure is slightly higher than the atmospheric pressure.

f) HEAT LOSSES. These are due to losses through conduction and radiation to the exterior. /61

g) MECHANICAL LOSSES. These occur in the bearings and in other mechanical systems.

Of the losses mentioned, the most important are those covered in points a, b, d, and e.

In order to observe the effects of losses more clearly, we will consider only the losses cited in points a and d, or losses in the compressor and turbine. The expression of yield is:

$$\eta_t = \frac{\eta_{\tau} \left(1 - \frac{1}{\pi^m}\right) - \frac{1}{\tau \eta_c} (\pi^m - 1)}{1 - \frac{1}{\tau} - \frac{1}{\tau \eta_c} (\pi^m - 1)}$$

where $\tau = T_3 / T_1$

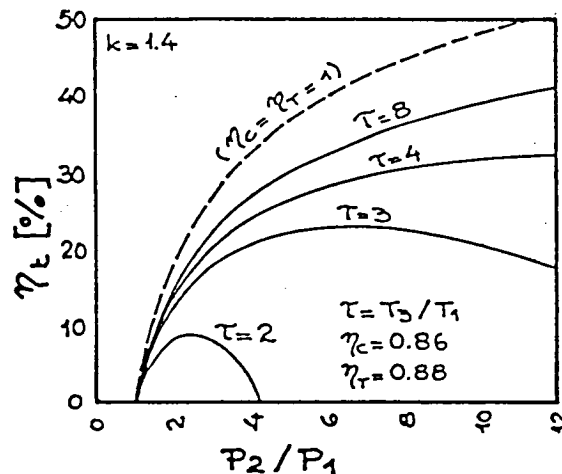


FIG. D YIELDS IN THE JOULE-BRAYTON CYCLE WITH LOSSES IN THE COMPRESSOR AND TURBINE

The variation of the total efficiency η_t for the particular case $\eta_c = 0.86$ and $\eta_{\tau} = 0.88$ is fulfilled as a function of P_2/P_1 and T_3/T_1 in Figure D. As a means of

comparison, the efficiency for the ideal cycle ($\eta_c = \eta_t = 1$) which does not depend on the temperature, was superimposed in dotted lines.

Note that, in the real cycle, not only the compression ratio is of interest but also the value of the hot temperature T_3 . Its elevation is a very efficient medium for improving the system's efficiency.

It is important to note that, in the real cycle, the efficiency does not increase monotonically with the compression ratio unless the existence of a favorable value (already fixed at T_3/T_1) is verified, from which the yield starts to decrease due to the effect of losses in the workings actually involved in the compressor and the turbine. / 62

The influence of the loss of pressure in the ducts and the compression chamber, as well as the existence of excess pressure in the outlet, is affecting the system, so that the efficiency of the turbine would be smaller. The yield formula expressed as a function of η_c and η_t is identical in this case. If η_t is replaced for $\eta_t \times \eta_r$ where:

$$\eta_r = \frac{1 - (P_3/P_4)^{-m}}{1 - (P_2/P_1)^{-m}}$$

The value of η_r expresses the ratio of power with and without losses in the ducts.

3.) JOULE-BRAYTON REGENERATIVE CYCLE

The Ideal Regenerative Cycle

Figure E shows a representation of the regenerative cycle in a T-S graph.

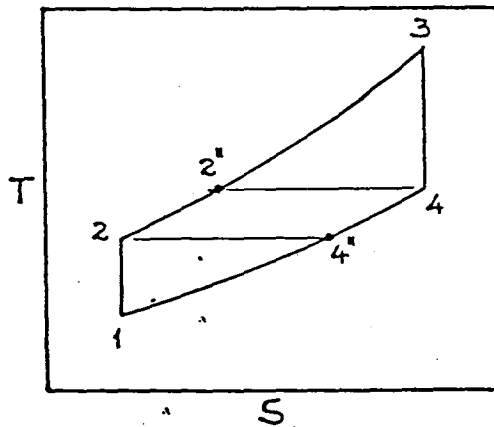


FIG. E REGENERATIVE JOULE-BRAYTON CYCLE

The path of the fluid is similar to that of the non-regenerative cycle. The difference is in how the isobaric heating is produced (2-3).

Since the outlet temperature of the outlet to the atmosphere is frequently very high in the non-regenerative /63 system, the amount of heat lost in the 4-1 process causes the cycle's low efficiency.

The objective of regeneration is to employ part of this heat to improve the efficiency. If a heat exchanger is placed at the outlet nozzle (point 4), before discharging the fluid to the atmosphere, and thermal energy is transferred to the air mass which exits from the compressor (before entering the combustion chamber), less fuel is required to reach point 3 of Figure E. A diagram of the motor is shown in Figure F.

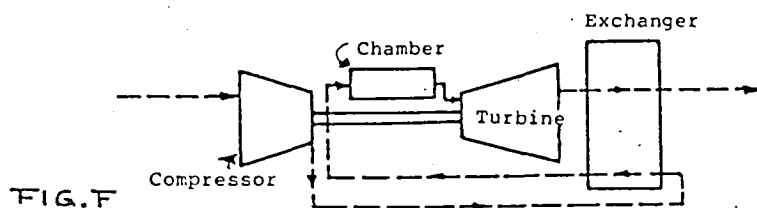


FIG. F

This procedure will be valid if $T_4 > T_2$, since otherwise there would not be usable energy, according to the second principle of thermodynamics.

Figure E shows that the amount of heat that can be transferred to the fluid leaving the compressor is:

$$Q = h_4 - h_{4''} \cong \bar{c}_p \cdot (T_4 - T_{4''})$$

This heat must be equal to the heat that the fluid to be heated can absorb. Its value is:

$$Q = h_{2''} - h_2 \cong \bar{c}_p \cdot (T_{2''} - T_2)$$

The resulting is that:

$$T_4 - T_{4''} = T_{2''} - T_2$$

The efficiency of the ideal regenerative cycle is:

$$\eta_t = 1 - \frac{\pi^m}{T}$$

Note the substantial change in the expression of efficiency when compared with the non-regenerative cycle: in

this case the increase in the compression ratio decreases the efficiency. It is also very dependent on the ratio T_3/T_1 , whose value did not at all change the efficiency of the non-regenerative cycle. /64

The cycle is ideal (and therefore cannot be achieved in practice) but it is important to note that, if the value of π tends toward 1, the efficiency tends toward the efficiency value of the Carnot cycle.

The influence of the compression ratio on the yield of the ideal cycle is shown in Figure G.

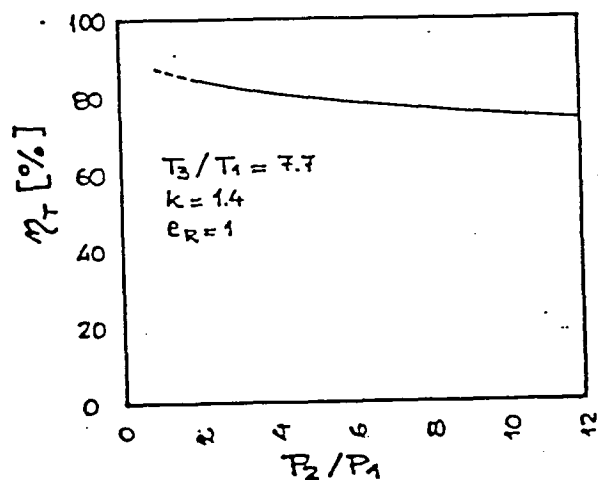


FIG G YIELD IN THE IDEAL CYCLE

In this case it was assumed that $T_3/T_4 = 7.7$

Regeneration Efficiency

Regeneration efficiency, e_r , can be defined as follows:

$$e_r = \frac{\text{Heat absorbed by air exiting the compressor}}{\text{Heat theoretically relinquished by the gas exiting the turbine}}$$

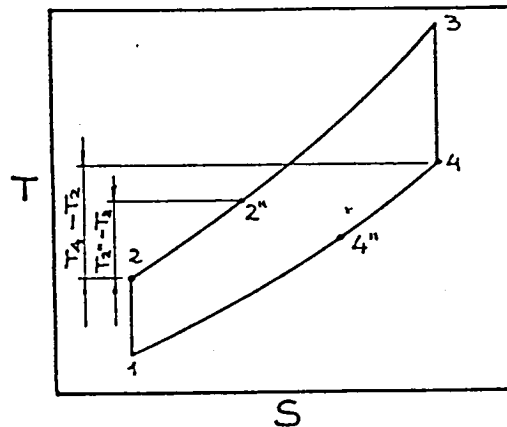
This means that:

$$e_r = \frac{h_2'' - h_2}{(1 + \lambda)(h_4 - h_2)} \quad \text{where } \lambda \text{ is the mass fuel/air ratio}$$

Considering that $C_p = \text{constant}$ and depreciating λ , the above expression is changed to:

$$e_r \cong \frac{T_2'' - T_2}{T_4 - T_2}$$

To find points 2, 2", 4, 4", refer to Figure H.



/65

FIG. H CYCLE WITH PARTIAL REGENERATION

In practice, the ideal regenerative cycle ($e_r = 1$) cannot be achieved since it would require a countercurrent heat exchanger with an unlimited energy transfer surface area.

The value of e_r is normally 0.75 and in certain special cases it can exceed the value of 0.90.

Considering the cycle, with a defined value of e_r and ignoring the other losses, the following efficiency results:

$$\eta_t = \frac{(1 - \frac{1}{\pi^m})(1 - \frac{\pi^m}{\tau})}{1 - \frac{\pi^m}{\tau} - e_r (\frac{1}{\pi^m} - \frac{\pi^m}{\tau})}$$

For $e_r = 0$, we obtain the efficiency of the ideal non-regenerative cycle:

$$\eta_t = 1 - \frac{1}{\pi^m}$$

For $e_r = 1$, we obtain:

$\eta_t = 1 - \frac{\pi^m}{\tau}$ which is the efficiency of the ideal regenerative cycle.

Obviously for intermediate values of e_r , an intermediate yield also results. The variation in the yield as a function of the variables τ, π, e_r can be observed in Figure I.

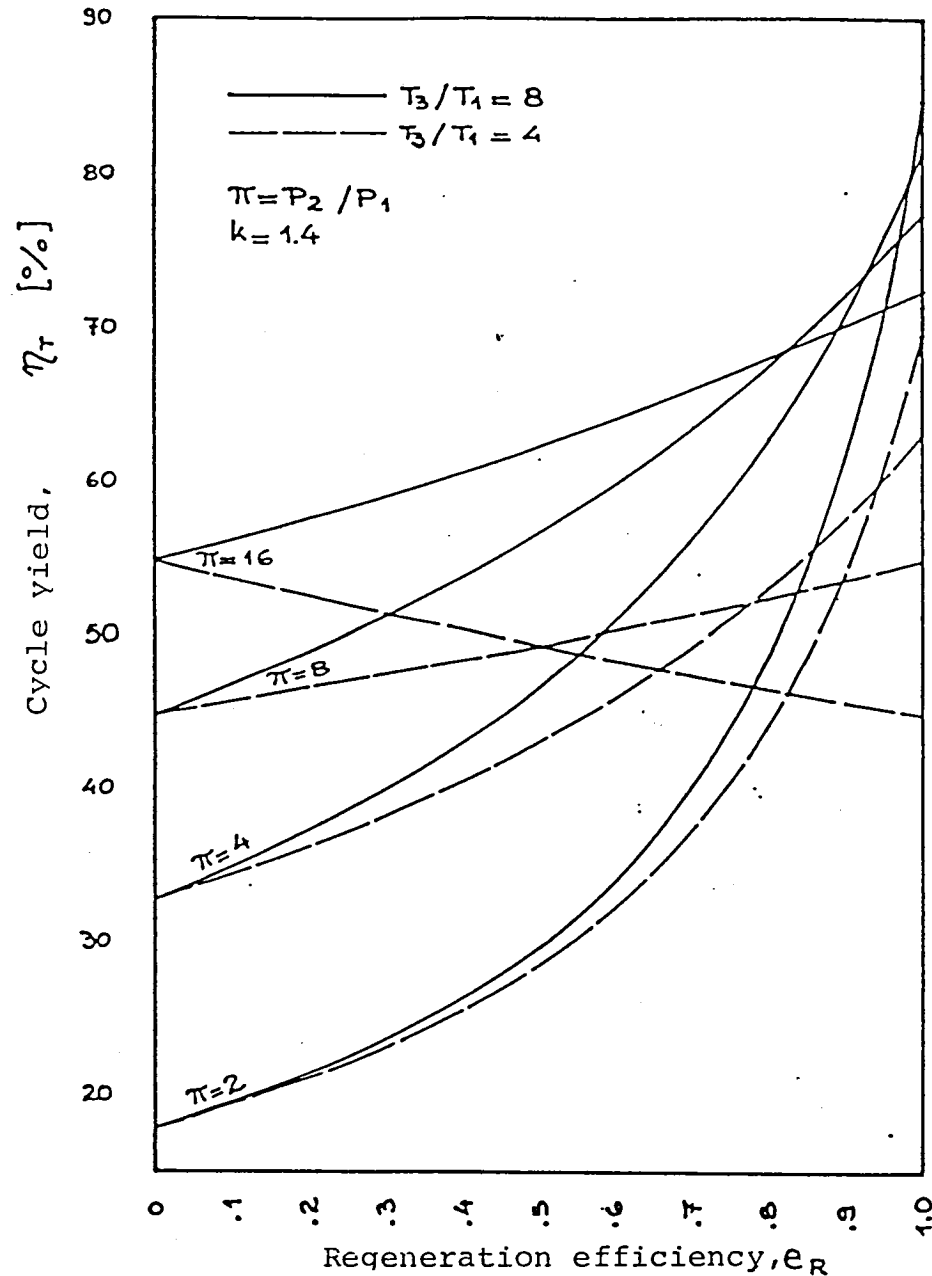


FIG. I YIELD OF THE JOULE-BRAYTON CYCLE WITH REGENERATION AS A FUNCTION OF ITS PRINCIPLE VARIABLES

It can be observed that, for low values of regeneration efficiency, the compression ratio has the greatest influence on efficiency. The value of T_3/T_4 is most important in increasing e_r , where it notably improves efficiency. The more efficient the regeneration, the lower the influence of the compression ratio.

Therefore, in actual practice if regeneration is high, the most profitable solution is to work with moderate compression ratios and the highest possible temperature from the combustion

chamber outlet.

Figure I shows that for a compression ratio of 16 and $\tau = 4$, the efficiency decreases with regeneration, due to the fact that in this case $T_4 < T_2$, and therefore the transfer of heat does little more than warm the outlet gases.

The result is that for each value of T_3/T_4 there exists a higher limit of P_2/P_1 , so that the location of the regenerator makes sense. This can be seen in Figure J.

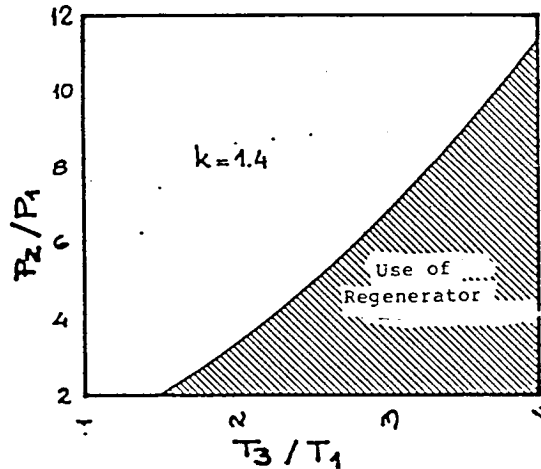


FIG. J COMPRESSION RATIOS AS A FUNCTION OF TEMPERATURE FOR THE UTILIZATION OF THE REGENERATOR

Figure K shows the importance of the compression ratio in the efficiency of the regenerative cycle for a fixed value of T_3/T_4 , and for different regeneration coefficients.

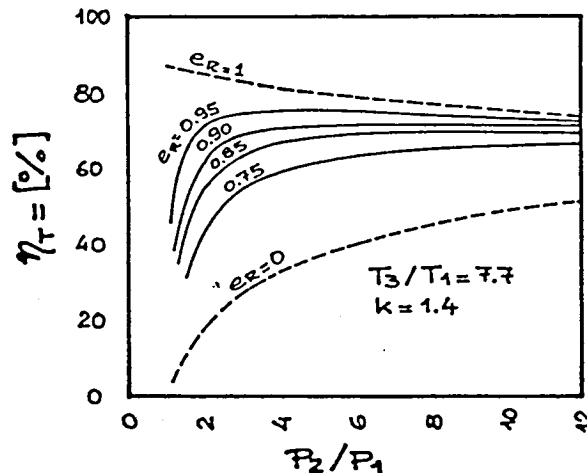


FIG. K YIELDS OF THE REGENERATIVE CYCLE FOR CERTAIN VALUES OF e_r

Once the efficiency is established, we can proceed to size the surface area through which the exchange of energy between the products of combustion and the air exiting the compressor will take place.

The basic equation of the regenerator is:

$$A = G \frac{e_R (h_4 - h_2'')}{k \cdot \Delta t}$$

where

- A = surface area of the regenerator
- G = mass volume of air
- k = total coefficient of heat transfer
- t = Difference in temperature between the two fluids which
- Δt = circulate in the regenerator

The approximate result is:

$$A = G \frac{\bar{c}_p}{k} \frac{e_R}{1 - e_R}$$

Figure L demonstrates how the necessary area increases as a function of the desired regeneration efficiency.

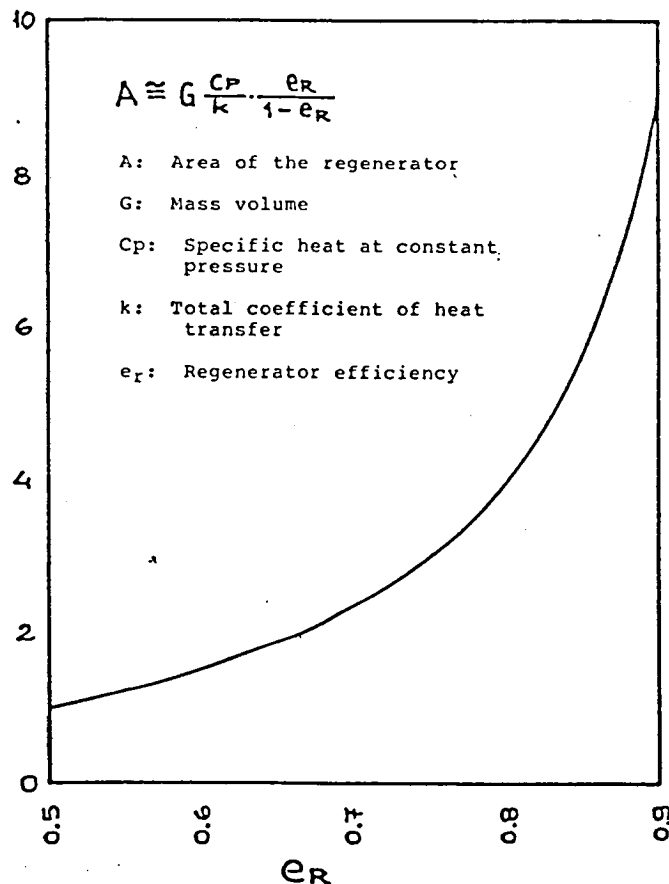


FIG. L SURFACE AREA OF THE REGENERATOR AS A FUNCTION OF ITS EFFICIENCY

4.) THE REAL JOULE-BRAYTON CYCLE WITH PARTIAL REGENERATION /69

The corresponding T-H graph is shown in Figure M. Not diagramming it as a T-S graph signifies that now the specific heat C_p is not considered constant with the temperature.

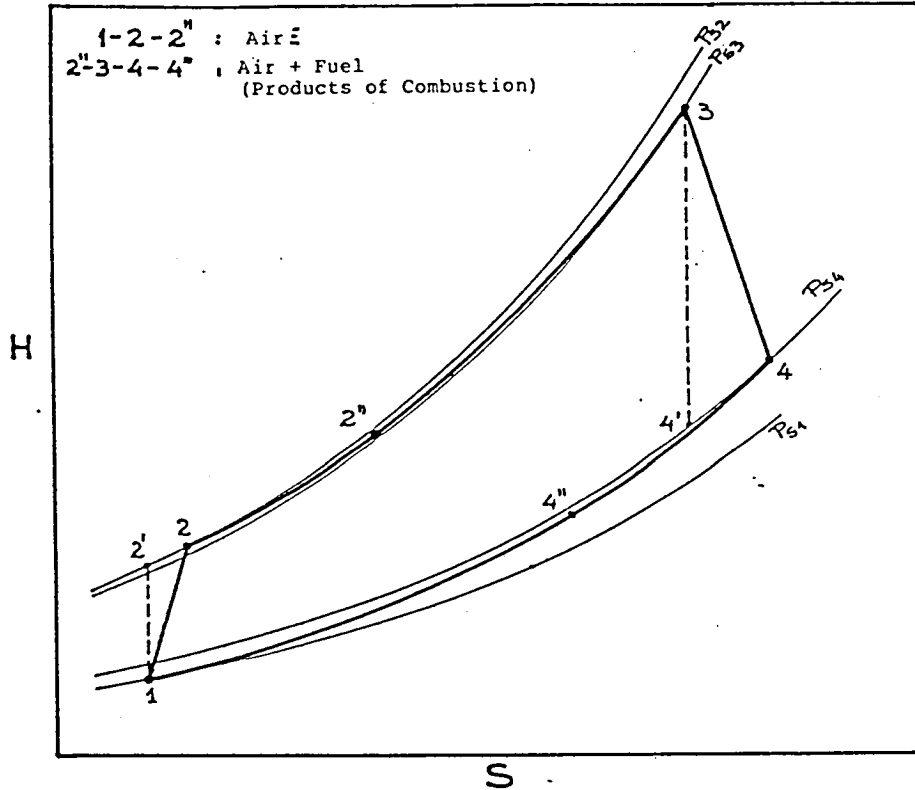


FIG. M REAL REGENERATIVE CYCLE

The same losses as in the simple real cycle (non-regenerative) have been considered, with the addition of a certain efficiency, e_r . The corresponding value of C_p must be used for the calculation of total heat, and this value must be corrected for the presence of combustion products, when they exist.

5.) RESOLUTION OF A PARTICULAR CASE

/70

Legend

- P = pressure
- T = temperature
- δ = density
- h = entalpy
- G = mass air volume
- A = Area
- λ = Air/fuel ratio

g = Acceleration of gravity
 V = Velocity
 k = Cp/Cv
 M = Mach number
 P.C. = Power supplied to the compressor
 η = Yield

Subindex

S = Static
 T = Total
 a = Air
 g = Gas (combustion product)

Assumptions

Compressor efficiency, $\eta_c = 0.86$
 Combustion efficiency, $\eta_{cc} = 0.98$
 Nozzle efficiency, $\eta_t = 0.95$
 Temperature, $T_3 = 4000^\circ\text{R}$
 Pressure drop, $\Delta P_{2-3}/P_2 = 4\%$
 Excess pressure, $\Delta P_{4-1}/P_1 = 10\%$
 Regenerator efficiency, $e_r = 0.75$
 Low heating power of fuel = 19090 BTU/lb
 Hydrogen/carbon ratio of fuel H/C = 0.183
 Pressure, $P_{s2} = 30$ psi

Initial Data

$P_{t1} = 14.7$ psi
 $T_{t1} = 520^\circ\text{R}$
 $V_1 = 100$ ft/sec.
 $P_{s1} = 14.6$ psi
 $T_{s1} = 519^\circ\text{R}$
 $h_{s1} = 28.6$ BTU/lb
 $R_a = 1716$ ft.²/sec.² °R = 0.3705 psi/(lb/ft.³) °R

/71

Calculations in the Compressor

The equations to be solved are:

$$T_2' = \left(\frac{P_{s1}}{P_{s2}} \right)^{\frac{1-k}{k}} \cdot T_{s1}$$

where $k = 1.41$

$$T_{s2} = T_{s1} + \frac{T_2' - T_{s1}}{\eta_c}$$

From Figure P (see "Additional Comments" in this Appendix) we obtain:

$$T_{s2} \Rightarrow h_{s2a}$$

Resulting in:

$T_2 = 640^\circ\text{R}$
 $T_{S2} = 660^\circ\text{R}$
 $h_{S2a} = 62.5 \text{ BTU/lb}$

Calculations for Point 3 and Combustion Without Regeneration (First Repetition)

The equations to be used are:

$$P_{S3} = \left(1 - \frac{\Delta P_{2,3}}{P_{S2}} \right) P_{S2} = 0.96 P_{S2}$$

$$\lambda = \frac{h_{3a} - h_{2a}}{\eta_{cc} H_c - h_{3a} - \psi_{h3}} \quad (\text{See "Additional Comments" section of this appendix.})$$

where h_{32} is obtained from Figure P beginning with the value of T_{S3} and ψ_{h3} is obtained from Figure Q (see "Additional Comments" section of this appendix) beginning with T_{S3} and from H/C.

$$h_{3g} = h_{3a} + \frac{\lambda}{1+\lambda} \psi_{h3}$$

Results:

$P_{S3} = 29.1 \text{ psi}$
 $h_{3a} = 1016 \text{ BTU/lb}$
 $\psi_{h3} = 1884 \text{ BTU/lb}$
 $\lambda = 0.06032$

Calculations for the Nozzle

/72

We are considering that there is no turbine; therefore all of the expansion 3-4 occurs in the nozzle in order to increase the velocity.

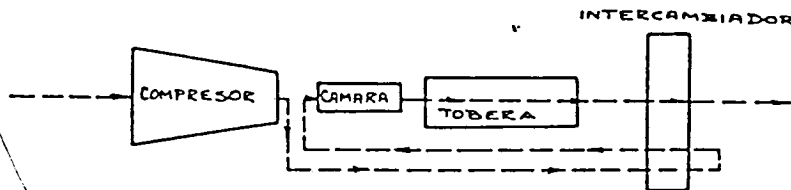


FIG. N

The following equations must be solved:

$$T_{S4'} = \left(\frac{P_{S3}}{P_{S4}} \right)^{\frac{1-k}{k}} T_{S3} \quad \text{where } k \cong 1.33$$

Assuming that the velocity V_3 is depreciable opposite V_4 , we can assume that:

$$\frac{T_{s4'}}{T_{T4}} = \frac{T_{s4'}}{T_{s3}}$$

From that equation we can obtain from tables the value of the Mach number of the fluid for $k = 1.33$.

The calculation of velocity V_4 can be done using:

$$V_4 = \sqrt{(h_3 - h_4) 2gJ + v_3^2}$$

To calculate h_4 we must first obtain the value of T_{s4} , which can be approximated by:

$$\eta_T = \frac{T_{s4} - T_{s3}}{T_4' - T_{s3}}$$

if we consider that C_p does not vary greatly between the temperatures considered. With the value T_{s4} we can obtain, by means of Figure P and Figure Q, the values of h_{4a} and ψ_{h4} h_4 . Therefore:

$$h_{4g} = h_{4a} + \frac{\lambda}{1 + \lambda} \psi_{h4}$$

Results:

$$\begin{aligned} T_4 &= 3438^\circ R \\ T_{s4} &= 3466^\circ R \\ M_4 &= 0.966 \\ h_{4a} &= 844 \text{ BTU/lb} \\ \psi_{h4} &= 1474 \text{ BTU/lb} \\ h_{4g} &= 928 \text{ BTU/lb} \\ V_4 &= 2996 \text{ ft./sec.} \end{aligned}$$

/73

by means of the equation

$$M_4 = V_4 / C_4$$

where

$$C_4 = \sqrt{k R_g T_{s4}}$$

An approximate value of R_g can be obtained.

Partial Conclusions

Up to now, the calculation corresponds to a non-regenerative cycle.

Its efficiency can be expressed as

$$\eta_t = \frac{(1 + \lambda)(h_{3g} - h_{4g})}{\lambda H_c}$$

For this case, $\eta_t = 17.96\%$

If we have as data a value of the available power to be supplied to the compressor, we can calculate the maximum air volume:

$$P.C. = G \cdot (h_{s2} - h_{s1})$$

$$\Rightarrow G = \frac{P.C.}{h_{s2} - h_{s1}}$$

Resulting, in our case, as:

$$G = \frac{1}{47.96} \frac{P.C.}{HP} \frac{lb}{seg}$$

The thrust obtained by the motor would be:

$$F = \frac{G}{g} \left[(1+\lambda)V_4 - 1 \cdot V_1 \right] + (P_{s4} - P_{s1}) \cdot A_4$$

Depreciating the result due to the excess pressure, we obtained:

$$F \cong 1.91 \frac{lb}{seg} \cdot \frac{P.C.}{HP}$$

Calculation of Regeneration (Successive Repetitions)

$$h_{2''} = e_R (1+\lambda)(h_{s4} - h_{s2}) + h_{s2}$$

$$h_{4''} = h_{s4} - \frac{h_{2''} - h_{s2}}{1+\lambda}$$

$$\lambda = \frac{h_{3a} - h_{2''}}{\eta_{cc} H_c - h_{3a} - \psi_{h3}}$$

$$h_{3g} = h_{3a} + \frac{\lambda}{1+\lambda} \psi_{h3}$$

$$h_{4g} = h_{4a} + \frac{\lambda}{1+\lambda} \psi_{h4}$$

These equations must be repeated until obtaining a stable value of .

Results:

$$h_{3g} = 1055 \text{ BTU/lb}$$

$$h_{4g} = 875 \text{ BTU/lb}$$

$$h_{2''} = 684 \text{ BTU/lb}$$

$$h_{4''} = 266 \text{ BTU/lb}$$

$$\lambda = 0.021 \text{ kg. of fuel/kg. of air}$$

/74

Complementary Calculations

Densities are calculated by using the state of perfect gases equation.

$$\rho_{si} = \frac{P_{si}}{R_i T_{si}}$$

We must now re-calculate:

$$V_4 = 3017 \text{ ft./sec.}$$

$$R_g = 2116 \text{ ft.}^2/\text{sec.}^2 \cdot \text{R} = 0.4567 \text{ psi}/(\text{lb}/\text{ft.}^3) \cdot \text{R}$$

Obtaining:

$$\rho_{s1} = 0.0759 \text{ lb}/\text{ft.}^3$$

$$\rho_{s2} = 0.1227 \text{ lb}/\text{ft.}^3$$

$$\rho_{s3} = 0.0159 \text{ lb}/\text{ft.}^3$$

$$\rho_{s4} = 0.0100 \text{ lb}/\text{ft.}^3$$

The resulting efficiency is:

$$\eta_t = \frac{1+\lambda}{\lambda} \cdot \frac{h_{3g}-h_{4g}}{H_c} = 45,84 \%$$

The drive will be:

$$F = 1,93 \overline{\text{lb}} \frac{\text{PC.}}{\text{HP}}$$

Summary of Results

/75

Point	P _s	T _s	ρ _s	h _s	S	V
	psi	°R	lb/ft ³	BTU/lb	BTU/lb°R	ft/seg
1	14,6	519	0,0759	28,6	0	100
2	30,0	660	0,1127	62,5	0,0073	50
2"	29,5	2945	0,0270	684	0,3614	50
3	29,1	4000	0,0159	1055	0,4670	300
4	15,8	3466	0,0100	875	0,4697	3020
4"	15,0	1445	0,0227	266	0,1758	3020

$$\lambda = 0,021$$

$$\eta_t = 46\%$$

$$F = 1,93 \overline{\text{lb}} \cdot \frac{\text{PC.}}{\text{HP}}$$

$$G = \frac{1}{47,96} \frac{\text{lb}}{\text{seg}} \frac{\text{PC.}}{\text{HP}}$$

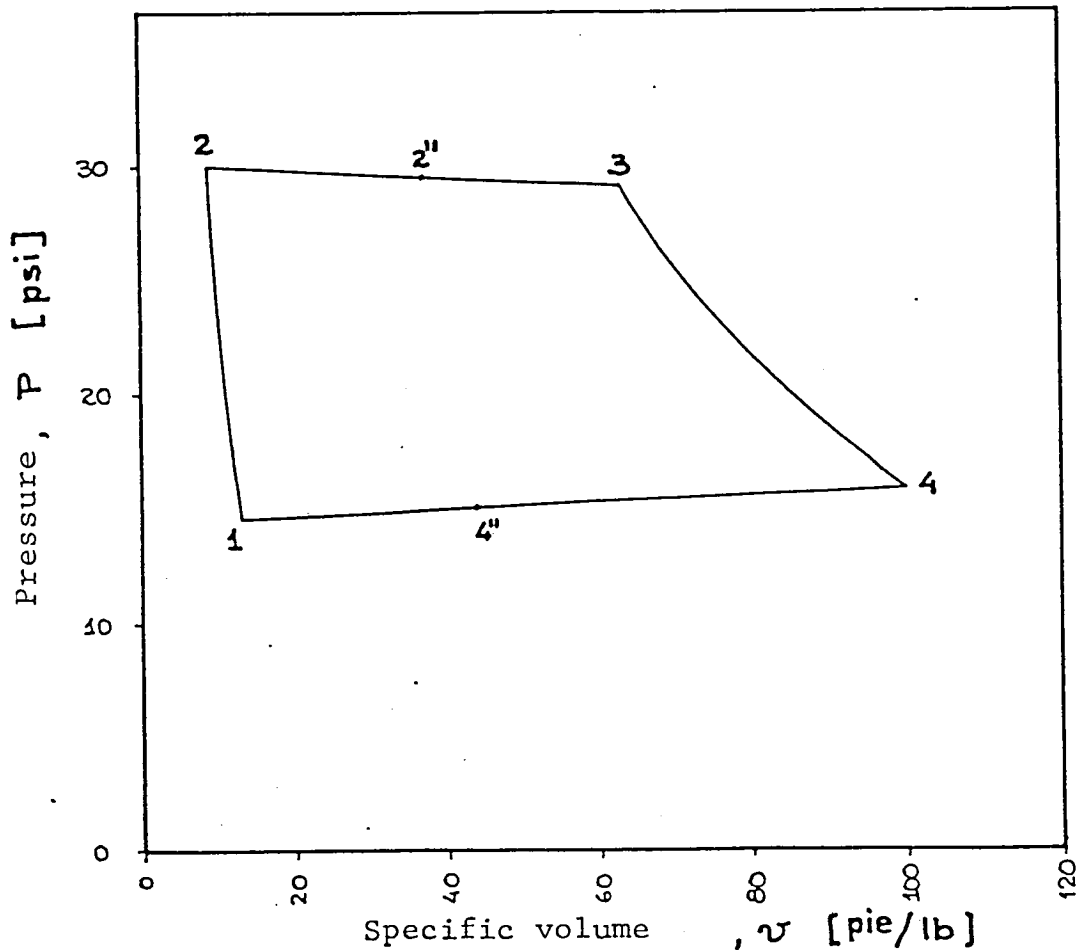


FIG. Oa CALCULATED CYCLE - DIAGRAM p-v

Conclusions

The ideal cycle, with $e_r = 0.75$, would have an efficiency of 53% taking into consideration the influence of the combustion products on the parameters of points 3, 4 and 4". The previously calculated cycle with the assumed loss hypotheses, has an efficiency of 86.8% with respect to the theoretical cycle.

It must be noted that the efficiencies previously calculated refer only to the fuel consumed. If the power supplied to the compressor is added, the value of η_t decreases:

$$\eta_t = 42.4\% \text{ instead of } 46.0\%$$

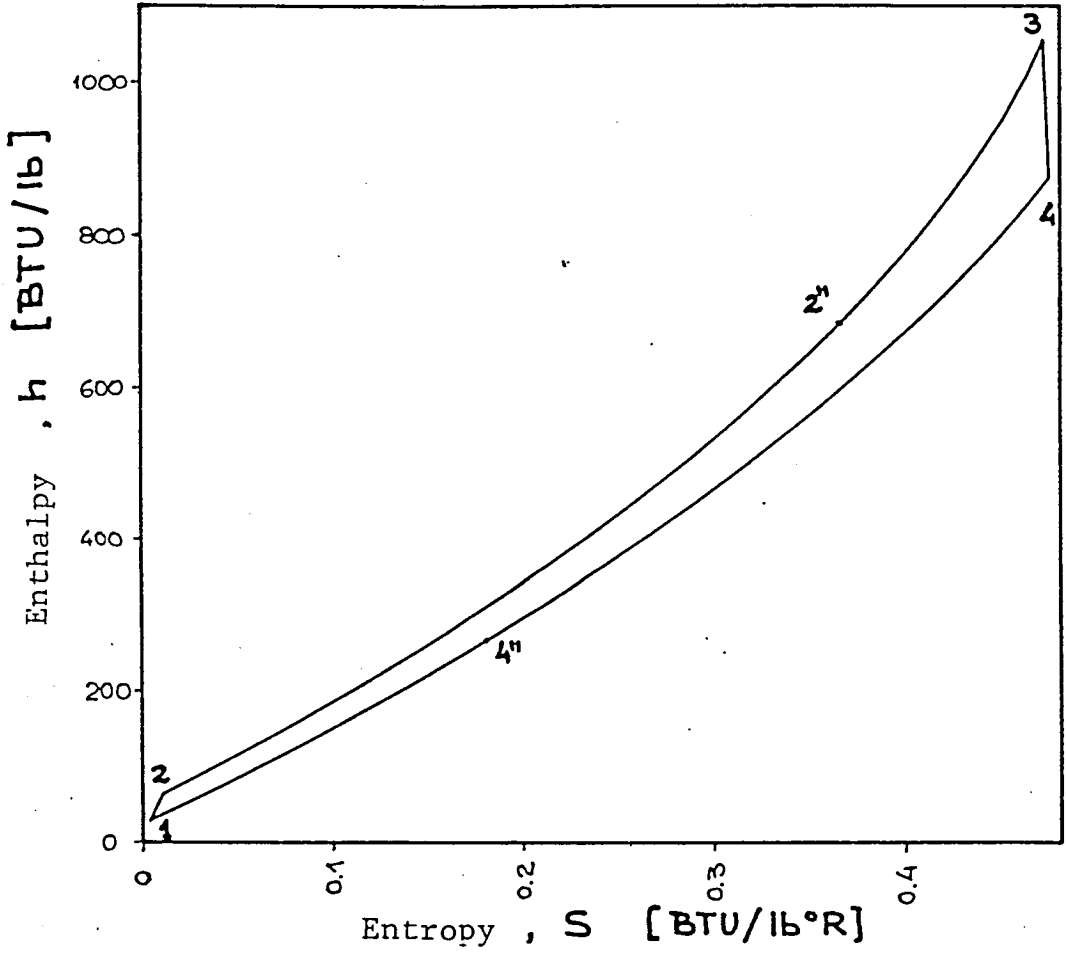


FIG. Ob CALCULATED CYCLE - DIAGRAM h-S

Additional Comments

The information necessary to calculate entalpy, air, and the products of combustion for the calculations in point 3 was not available.

The only data used was a table listing the thermodynamic properties of dry air from 400°R to 2500°R. By adjusting one parabola of the information obtained from the table by the least square method, the following equation was obtained: /77

$$h_a = 1.3445 \times 10^{-5} \times T^2 + 0.2233 \times T - 91$$

where [h_a] = BTU/lb
 [T] = °R

The test of the validity of the adjustment χ^2 gave a totally acceptable level of reliability:

$$\chi^2 = 0.0064 \quad 5.7$$

The value of 5.7 corresponds to a reliability of 99.5%. Figure P shows the graph resulting from the adjustment.

Chapter 19 of the book, "Thermal Turbo-engines" by Carlos Mataix, deals with the topic of combustion. It suggests methods of correcting enthalpy through combustion products. One of these refers to the Ψ_h function.

Figure 19-2 of section 19.1.5.1 diagrams the value of Ψ_h as a function of the H/C fuel ratio for values between 0.15 and 0.20, and as a function of temperature up to 1650°C. Since higher values (2950°C = 4000°R) required data on Ψ_h , it was necessary to estimate information in this case, also. The data contained in figure 9-2 mentioned above were modified, and the H/C = 0.15 and 0.20 curves were again adjusted by the parabolic least square method. A lineal interpolation must be realized for intermediate values of H/C.

Following are the equations to be used in calculating the cycle using the correction method of the function Ψ_h , according to the book mentioned above:

$$\begin{aligned} h_g &= h_a + \frac{\lambda}{1+\lambda} \Psi_h \\ \lambda &= \frac{h_{a3} - h_{a2}}{\eta_{cc} H_c - h_{a3} - \Psi_h} \end{aligned}$$

The curves resulting from the adjustment mentioned are:

$$H/C = 0,15 \Rightarrow \Psi_h = 4,546 \times 10^{-4} \times T^2 + 1,126 \times T - 104,7$$

$$H/C = 0,20 \Rightarrow \Psi_h = 5,552 \times 10^{-4} \times T^2 + 1,366 \times T - 112,7$$

where $[\Psi_h] = \text{kJ/kg} = 2.3258 \text{ BTU/lb}$
 $[T] = ^\circ\text{C}$

Tests of the validity of the adjustment χ^2 , confirmed reliability ratings greater than 99.5%. This is why it was considered possible to estimate data.

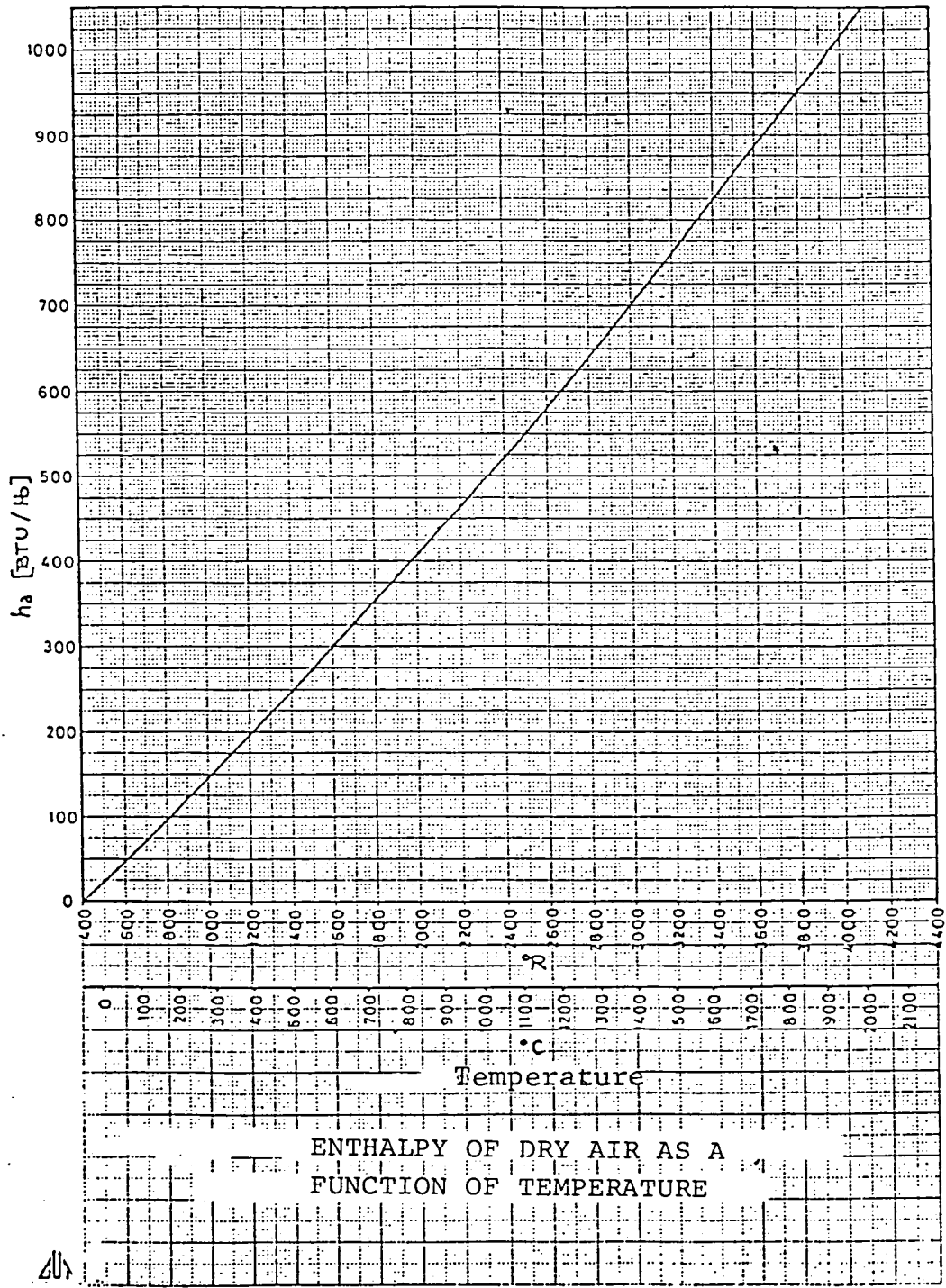


FIG. P ENTALPY OF DRY AIR AS A FUNCTION OF TEMPERATURE

Figure Q shows the tendencies of the two adjusted curves.

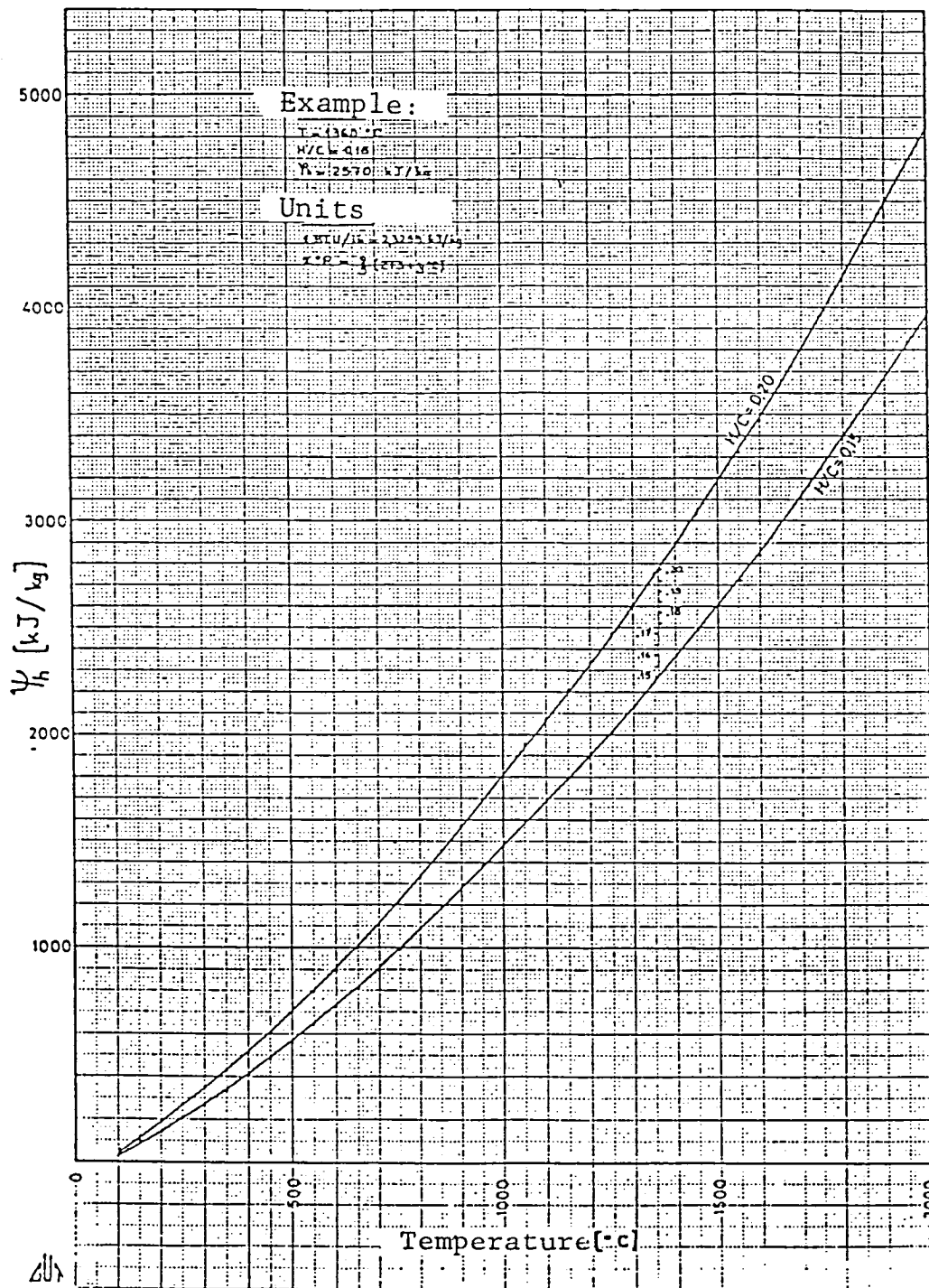
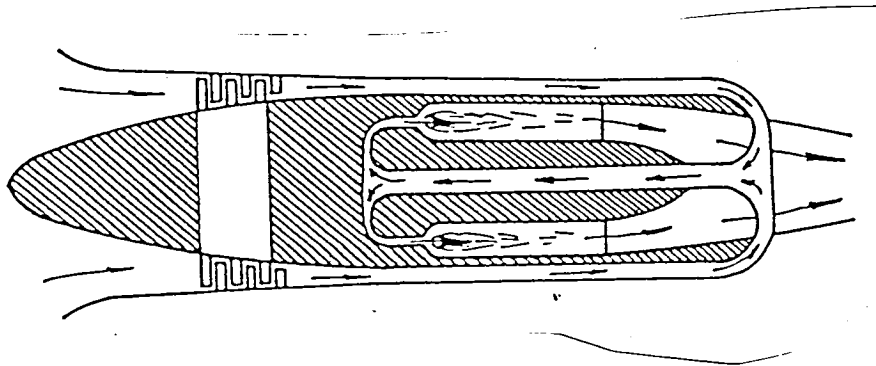


FIG. Q FUNCTION Ψ_h , DEPENDING ON TEMPERATURE AND ON H/C

Other Results

The particular case studied above corresponds with the following drawing (Figure R).



/80

FIG. R

Other cases have been resolved where an external source of power supply to the compressor was assumed (no turbine) and where the excess pressure (ΔP_{4-1}) was considered to be in proportion to the pressure drop in the nozzle.

The initial conditions and the loss hypotheses were assumed to be the same. Figure S shows the results:

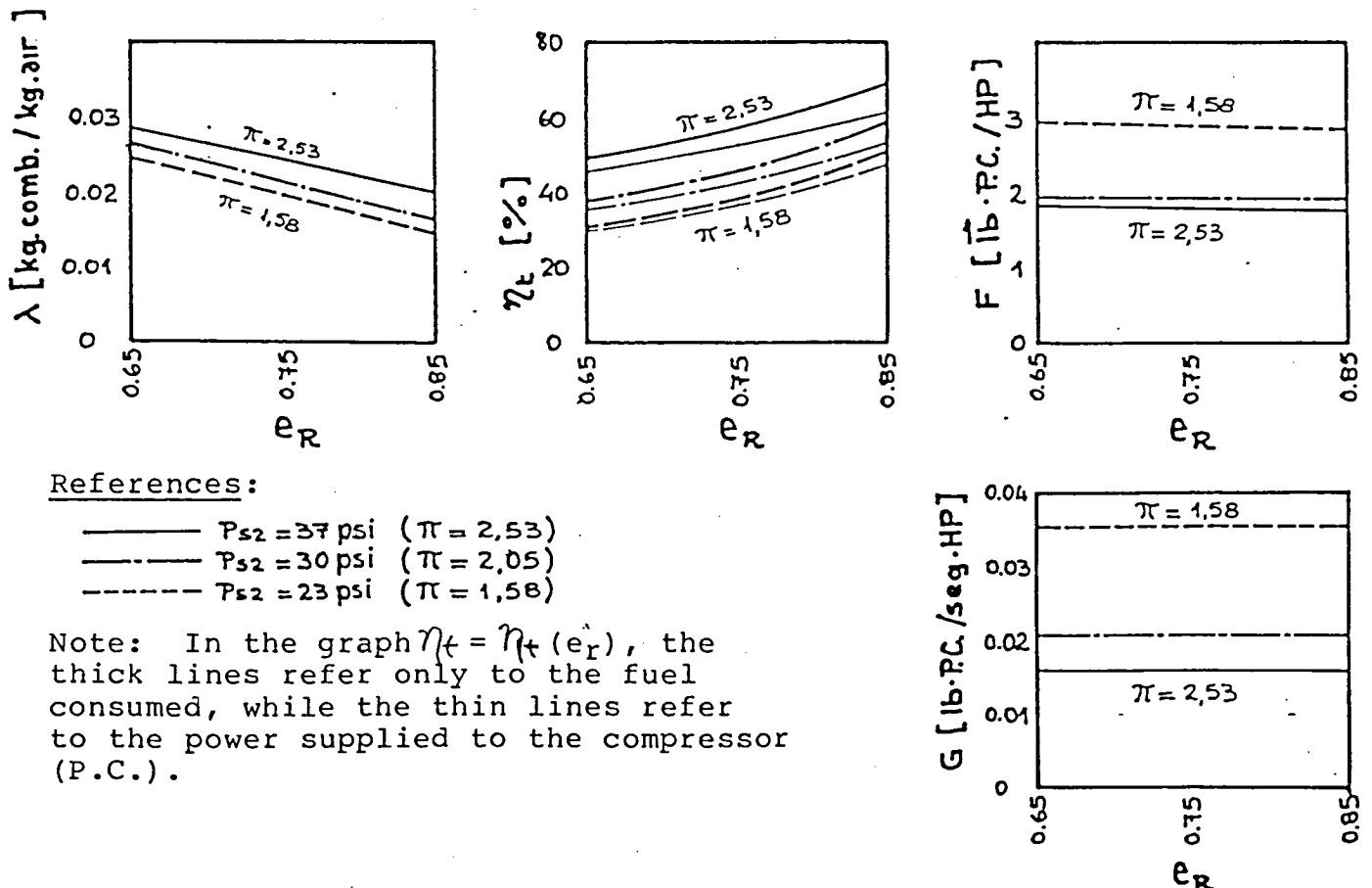


FIG. S PARAMETERS OF DIVERSE CYCLES

72

It is important to note that for a greater compression /81 ratio, the efficiency of the cycle is greater, but the power drive supplied to the compressor is lower, since the drive diagram as a function of regeneration is closely associated with the air volume which circulates through the system, while the efficiency of the cycle is independent of it. Therefore, for a given compressor power, if the increase of pressure is lower, then the air volume must be greater.

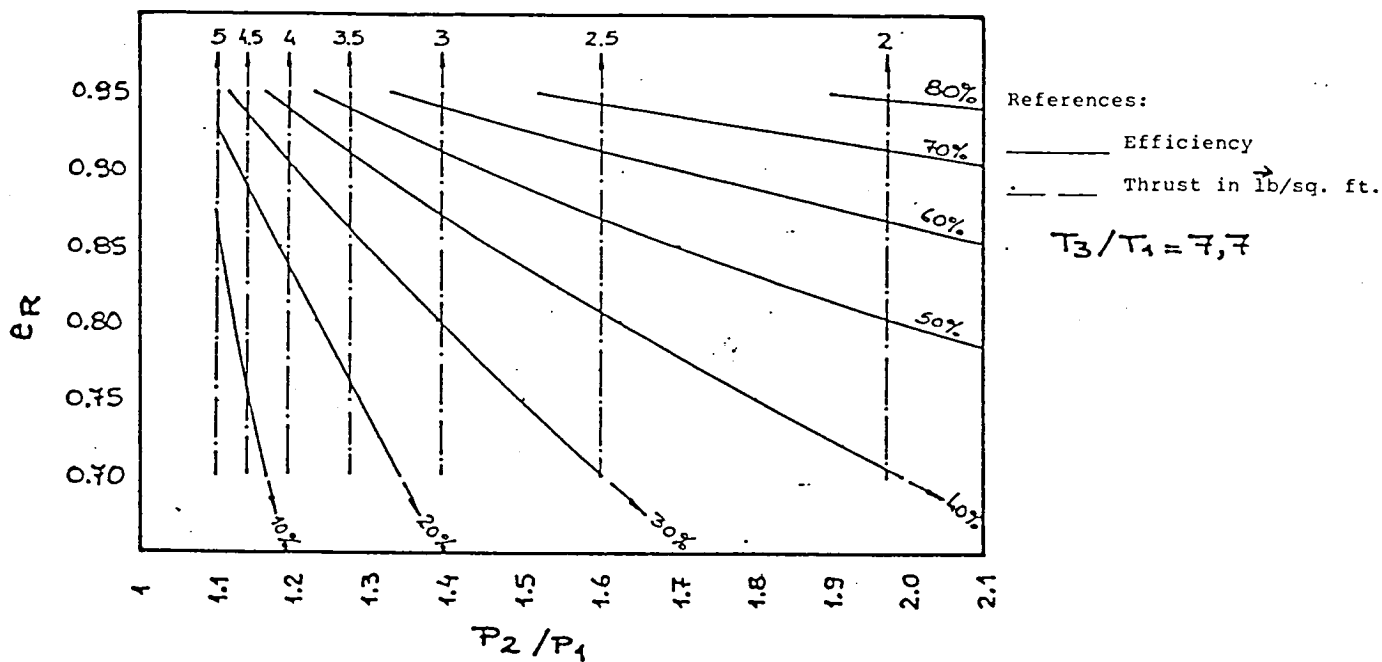


FIG. T PERFORMANCE OF THE PROPOSED DIAGRAM. Note: The calculations for this figure were simplified as compared to previous calculations.

- Aplicaciones de la energia solar [Applications of Solar energy] (A. B. Meinel - M. P. Meinel).
- Fisica, Parte II [Physics, Part II] (Halliday-Resnick)
- Trabajos Practicos, Fisica III [Practical Studies, Physics III] (U.B.A.).
- Silicon Solar Cell Arrays: Technical status, terrestrial applications and future development for low cost production (R. Buhs - AEG Telefunken)
- Datos Tecnicos [Technical Data] (AEG Telefunken).
- The Role of Research and Development in the Worldwide Deployment of Photovoltaics (J. Stone - D. Ritchie, S. Deb - T. Surek)
- A New High-Efficiency GaAs Solar Cell Structure (R. Gale - J. Fan - G. Turner - R. Chapman).
- Solar Challenger - "FLAPS" Magazine.
- Sun-Powered Aircraft Designs (P. MacCready - P. Lissaman W. Morgan - J. Burke).
- Energy - Special Report (National Geographic).
- Mission Analysis of Solar Powered Aircraft (D. Hall D. Watson - R. Tuttle - S. Hall).
- Turboreactors (A. Oñate)
- Turbomaquinas termicas [Thermal turbo-engines] (C. Mataix).
- Ceramica en los motores de avion [Ceramics in aircraft motors] - "La Prensa"
- Apuntes y textos de Termodinamica [Notes and Texts on Thermodynamics].

LANGLEY RESEARCH CENTER



3 1176 00188 8776